

Experimentally Verifiable $U(1)_{B-L}$ Symmetric Model with Type-II Seesaw and Dark Matter

Purusottam Ghosh,^{1,*} Satyabrata Mahapatra,^{2,†}

Nimmala Narendra,^{3,‡} and Narendra Sahu^{2,§}

¹*Regional Centre for Accelerator-based Particle Physics,*

Harish-Chandra Research Institute, HBNI,

Chhatnag Road, Jhansi, Allahabad - 211 019, India

²*Department of Physics, Indian Institute of Technology Hyderabad,*

Kandi, Sangareddy 502285, Telangana, India

³*Theoretical Physics Division, Physical Research Laboratory, Ahmedabad 380009, India*

Abstract

In an endeavor to explain the light neutrino masses and dark matter (DM) simultaneously, we study a gauged $U(1)_{B-L}$ extension of the standard model (SM). The neutrino masses are generated through a variant of type-II seesaw mechanism in which one of the scalar triplets has a mass in a scale that is accessible at the present generation colliders. Three right chiral fermions $\chi_{iR}(i = e, \mu, \tau)$ with $B-L$ charges $-4, -4, +5$ are invoked to cancel the $B-L$ gauge anomalies and the lightest one among these three fermions becomes a viable DM candidate as their stability is guaranteed by a remnant Z_2 symmetry to which $U(1)_{B-L}$ gauge symmetry gets spontaneously broken. Interestingly in this scenario, the neutrino mass and the co-annihilation of DM are interlinked through the breaking of $U(1)_{B-L}$ symmetry. Apart from giving rise to the observed neutrino mass and dark matter abundance, the model also predicts exciting signals at the colliders especially regarding the discovery of the triplet scalar in presence of the $B-L$ gauge boson. We see a $(34 - 54)\%$ enhancement in the production of the TeV scale doubly charged scalar in presence of the Z_{BL} gauge boson in a mass range 2.5 TeV to 4.4 TeV. We discuss all the relevant constraints on model parameters from observed DM abundance and null detection of DM at direct and indirect search experiments as well as the constraints on the $B-L$ gauge boson from recent colliders.

*Electronic address: purusottamghosh@hri.res.in

†Electronic address: ph18resch11001@iith.ac.in

‡Electronic address: mnarendra@prl.res.in

§Electronic address: nsahu@phy.iith.ac.in

I. INTRODUCTION

Out of all the lacunae afflicting the Standard Model(SM) of particle physics, the identity of DM and the origin of tiny but nonzero neutrino masses are the most irking ones. It is well established by now, thanks to numerous irrefutable observational evidences from astrophysics and cosmology like galaxy rotation curves, gravitational lensing, Cosmic Microwave Background (CMB) acoustic oscillations etc. [1–6], that a mysterious, non-luminous and non-baryonic form of matter exists called as dark matter (DM) which constitutes almost 85% of the total matter content and around 26.8% of the total energy density of the present Universe. In terms of density parameter $h = (\text{Hubble Parameter})/(100 \text{ km s}^{-1}\text{Mpc}^{-1})$, the present DM abundance is conventionally reported as [5, 6]

$$\Omega_{\text{DM}}h^2 = 0.120 \pm 0.001 \quad (1)$$

But still we have no answer to the question what DM actually is, as none of the SM particle has the properties that of a DM particle is expected to have. Thus over the years, various beyond SM (BSM) scenarios have been considered to explain the puzzle of DM, with additional field content and augmented symmetry. The most popular among these ideas is something known as the weakly interacting massive particle (WIMP) paradigm. In this WIMP scenario, a DM candidate typically having a mass similar to electroweak (EW) scale and interaction rate analogous to EW interactions can give rise to the correct DM relic abundance, an astounding coincidence referred to as the *WIMP Miracle* [7, 8]. The sizeable interactions of WIMP DM with the SM particles has many phenomenological implications. Along with giving the correct relic abundance of DM through thermal freeze-out, it also leads to other phenomenological implications like optimistic direct and indirect detection prospects of DM which makes it more appealing. Several direct detection experiments like LUX, PandaX-II and XENON1T [9–13] and indirect detection experiments like space based telescopes Fermi-LAT and ground based telescopes MAGIC [14, 15] have been looking for signals of DM and have put constraints on DM-nucleon scattering cross-sections and DM annihilation cross-section to SM particles respectively.

Apart from the identity of DM, another appealing motivation for the BSM is the origin of neutrino masses. Despite compelling evidences for existence of light neutrino masses, from various oscillation experiments [16–20] and cosmological data [21–24], the origin of light neutrino masses is still unknown. The oscillation data is only sensitive to the difference in

mass-squareds[21, 25], but the absolute mass scale is constrained to $\sum_i |m(\nu_i)| < 0.12$ eV [21] from cosmological data. This also implies that we need new physics in BSM to incorporate the light neutrino masses as the Higgs field, which lies at the origin of all massive particles in the SM, can not have any Yukawa coupling with the neutrinos due to the absence of its right-handed counterpart.

Assuming that the neutrinos to be of Majorana type (which violates lepton number by two units), the origin of the tiny but non-zero neutrino mass is usually explained by the see-saw mechanisms (Type-I [26–29], Type-II [30–34] and Type-III [35]) which are the ultraviolet completed realizations of the dimension five Weinberg operator $\mathcal{O}_5 = y_{ij} \frac{\bar{L}_i L_j^c H H}{\Lambda}$, where L and H are the lepton and Higgs doublets of the SM and Λ is the scale of new physics [36, 37]. In the type-I seesaw heavy singlet RHNs are introduced while in type-II and type-III case, a triplet scalar(Δ) of hyper-charge 2 and triplet fermions Σ of hyper-charge 0 are introduced respectively such that new Yukawa terms can be incorporated in the theory. Tuning the Yukawa coupling and the cut-off scale (Λ) and adopting a necessary structure for the mass matrix, the correct masses and mixings of the neutrinos can be obtained.

In the conventional type-II seesaw, the relevant terms in the Lagrangian violating lepton number by two units are $f_{ij} \Delta L_i L_j + \mu \Delta^\dagger H H$, where Δ does not acquire an explicit vacuum expectation value(vev). However, after the electro-weak phase transition, a small induced vev of Δ can be obtained as: $\langle \Delta \rangle = -\frac{\mu \langle H \rangle^2}{M_\Delta^2}$. Thus for $\mu \sim M_\Delta \sim 10^{14}$ GeV, one can get $M_\nu = f \langle \Delta \rangle \simeq f \frac{\langle H \rangle^2}{M_\Delta}$ of order $\mathcal{O}(0.1)$ eV for $f \sim 1$. But such models lack verifiability as the mass scale of the scalar triplet is much larger than the energy attainable at current generation colliders.

In an alternative fashion, neutrino mass can be generated in a modified type-II seesaw if one introduces two scalar triplets: Δ and ξ with $M_\Delta \sim 10^{14}$ GeV and $M_\xi \sim \text{TeV} \ll M_\Delta$ [38]¹. In this case imposition of additional B – L gauge symmetry [40] allows for $\mu \Delta^\dagger H H + f \xi L L + y \Phi_{\text{BL}}^2 \Delta^\dagger \xi$ terms in the Lagrangian (with proper choice of gauge charges for the scalars) where Φ_{BL} is the scalar field responsible for B – L symmetry breaking at TeV scale. As is clear from the Lagrangian terms, once the Φ_{BL} acquires a vev, it creates a small mixing between Δ and ξ of the order $\theta \sim \frac{\langle \Phi_{\text{BL}} \rangle^2}{M_\Delta^2} \simeq 10^{-18}$. Thus the coupling of ξ with Higgs becomes extremely suppressed but $\xi L L$ coupling can be large. In this scenario,

¹ See also ref. [39] for a modified double type-II seesaw with TeV scale scalar triplet

Δ being super heavy gets decoupled from the low energy effective theory but ξ can have mass from several hundred GeV to a few TeV and having large Di-lepton coupling can be probed at colliders through the same sign Di-lepton signature [41–47].

If this type-II seesaw framework is implemented in a gauged $U(1)_{B-L}$ symmetric model, then one needs to invoke additional fields to make the model anomaly free as gauging the $U(1)_{B-L}$ introduces non-trivial gauge and gravitational anomalies. With only the SM particle content all triangle anomalies in the gauged B–L theory vanishes except for $\sum[U(1)_{B-L}]^3 = 3$ and $\sum[Grav.]^2 \times [U(1)_{B-L}] = 3$. Thus the only way to cancel these anomalies is by introducing new fermions in such a way that sum of their B – L quantum numbers is -3 . In this paper we adopt the choice of $U(1)_{B-L}$ charges $-4, -4, +5$ for three right chiral fermions χ_{i_R} ($i = e, \mu, \tau$) introduced for anomaly cancellation, such that $\sum_{i=1}^3 (Y_{B-L})_i = -3$ [48–58]. For the details of the anomaly cancellation in a B – L model, please see appendix A. Interestingly, the lightest one among these three exotic fermions becomes a viable candidate of DM, thanks to the remnant \mathcal{Z}_2 symmetry after $U(1)_{B-L}$ breaking, under which χ_{i_R} ($i = e, \mu, \tau$) are odd while all other particles are even.²

The origin of neutrino mass and DM is hitherto not known. Any connection between them is also not established yet. However, it will really be interesting if neutrino mass and the DM phenomenology have an inter-connection between them. In light of this, it is worth mentioning here that the framework we considered in this paper, the spontaneous breaking of $U(1)_{B-L}$ gauge symmetry via the vev of Φ_{BL} not only generates sub-eV masses of light neutrinos, but also give rise to co-annihilations among the dark fermions which in turn allows a larger parameter space in contrast to the gauged B – L models with right-handed neutrino DM giving rise required relic only at the Z_{B-L} -resonance [56, 60–62].

The rest of the paper is organized as follows. In section II, we describe the proposed model, the neutrino mass generation through a variant of type-II seesaw, the scalar masses and mixing. We then discuss how the particles introduced for anomaly cancellation become viable DM candidate and study the relic density in section III. In section IV, we studied all the relevant constraints from direct, indirect search of DM on our parameter space as well as scrutinized it with respect to the constraint from colliders. We briefly summarize

² Right handed neutrinos with B – L charge -1 can also serve the purpose of B – L anomaly cancellation and be viable DM candidate provided one introduces an additional ad hoc \mathcal{Z}_2 symmetry to guarantee their stability. For instance see [59, 60]

the collider search strategies of the model in section V and finally conclude in section VI.

II. THE MODEL

Fields		$\underbrace{SU(3)_C \otimes SU(2)_L \otimes U(1)_Y}_{\text{SM}} \otimes U(1)_{B-L}$			
Exotic Fermions	χ_{e_R}, χ_{μ_R}	1	1	0	-4
	χ_{τ_R}	1	1	0	5
Heavy Scalars	$\Delta = \begin{pmatrix} \frac{\delta^+}{\sqrt{2}} & \delta^{++} \\ \delta^0 & -\frac{\delta^+}{\sqrt{2}} \end{pmatrix}$	1	3	2	0
	Φ_{BL}	1	1	0	-1
	Φ_{12}	1	1	0	8
Light Scalars	$\xi = \begin{pmatrix} \frac{\xi^+}{\sqrt{2}} & \xi^{++} \\ \xi^0 & -\frac{\xi^+}{\sqrt{2}} \end{pmatrix}$	1	3	2	2
	Φ_3	1	1	0	-10

TABLE I: Charge assignment of BSM fields under the gauge group $\mathcal{G} \equiv \mathcal{G}_{\text{SM}} \otimes U(1)_{B-L}$, where $\mathcal{G}_{\text{SM}} \equiv SU(3)_C \otimes SU(2)_L \otimes U(1)_Y$.

In this work, the model under consideration is a very well motivated BSM framework based on the gauged $U(1)_{B-L}$ symmetry [63–67] in which we implement a modified type-II seesaw to explain the sub-eV neutrino mass by introducing two triplet scalars Δ and ξ . Δ is super heavy with $M_\Delta \sim 10^{14}$ GeV and $M_\xi \sim \text{TeV} \ll M_\Delta$ and the $B-L$ charges of Δ and ξ are 0 and 2 respectively. As already discussed in the previous section, the additional $U(1)_{B-L}$ gauge symmetry introduces $B-L$ anomalies in the theory. And to cancel these $B-L$ anomalies we introduce three right chiral fermions χ_{i_R} ($i = e, \mu, \tau$), where the $B-L$ charges of χ_{e_R}, χ_{μ_R} and χ_{τ_R} are -4, -4, +5 respectively. Note that such unconventional $B-L$ charge assignment of the χ_{i_R} ($i = e, \mu, \tau$) forbids their Yukawa couplings with the SM particles. Also three singlet scalars: Φ_{BL} , Φ_{12} and Φ_3 with $B-L$ charges -1, +8, -10 are introduced. As a result of which Φ_{12} and Φ_3 couples to χ_{e_R, μ_R} and χ_{τ_R} respectively

through Yukawa terms and the vevs of Φ_{12} and Φ_3 provides Majorana masses to these exotic fermions. The vev of Φ_{BL} provides a small mixing between Δ and ξ which plays a crucial role in generating sub-eV masses of neutrinos. This vev $\langle \Phi_{BL} \rangle$ is also instrumental in controlling the co-annihilations among the dark sector particles and hence is crucial for DM phenomenology too. As a consequence this establishes an interesting correlation between the neutrino mass and DM. The particle content and their charge assignments are listed in Table.I.

The Lagrangian involving the BSM fields consistent with the extended symmetry is given by:

$$\mathcal{L} = \mathcal{L}^{\text{SM+BSM Scalar}} + \mathcal{L}^{\text{DM}} \quad (2)$$

where

$$\begin{aligned} \mathcal{L}^{\text{SM+BSM Scalar}} \supset & |D_\mu H|^2 + |D_\mu \Phi_3|^2 + |D_\mu \Phi_{BL}|^2 + |D_\mu \Phi_{12}|^2 \\ & + \text{Tr}[(D_\mu \Delta)^\dagger (D^\mu \Delta)] + \text{Tr}[(D_\mu \xi)^\dagger (D^\mu \xi)] \\ & - Y_{ij}^\xi \bar{L}_i^c i\tau_2 \xi L_j \\ & - V^{\mathbb{L}}(H, \xi, \Phi_3) - V^{\mathbb{H}}(\Delta, \Phi_{BL}, \Phi_{12}) - V^{\mathbb{LH}}. \end{aligned} \quad (3)$$

Here i, j runs over all three lepton generations. In the above Lagrangian, $V^{\mathbb{L}}$ is the scalar potential involving scalars in sub-TeV mass range (H, ξ, Φ_3) , $V^{\mathbb{H}}$ stands for scalar potential of the heavy fields $(\Delta, \Phi_{BL}, \Phi_{12})$ and the scalar potential which involves both sub-TeV and super heavy fields is defined by $V^{\mathbb{LH}}$.

The covariant derivatives for these fields can be written as:

$$\begin{aligned} D_\mu H &= \partial_\mu H + igT^a W_\mu^a H + ig'B_\mu H \\ D_\mu F &= \partial_\mu F + ig[T^a W_\mu^a, F] + ig'Y B_\mu F + ig_{BL} Y_{BL} (Z_{BL})_\mu F & \text{where } F = \{\xi, \Delta\} \\ D_\mu G &= \partial_\mu G + ig_{BL} Y_{BL} (Z_{BL})_\mu G & \text{where } G = \{\Phi_3, \Phi_{BL}, \Phi_{12}\}. \end{aligned}$$

The Lagrangian of the dark sector can be written as:

$$\begin{aligned} \mathcal{L}^{\text{DM}} &= \overline{\chi_{e_R}} i\gamma^\mu D_\mu \chi_{e_R} + \overline{\chi_{\mu_R}} i\gamma^\mu D_\mu \chi_{\mu_R} + \overline{\chi_{\tau_R}} i\gamma^\mu D_\mu \chi_{\tau_R} \\ &+ Y_{11} \Phi_{12} (\overline{\chi_{e_R}})^c \chi_{e_R} + Y_{22} \Phi_{12} (\overline{\chi_{\mu_R}})^c \chi_{\mu_R} + Y_{12} \Phi_{12} (\overline{\chi_{e_R}})^c \chi_{\mu_R} \\ &+ Y_{13} \Phi_{BL} (\overline{\chi_{e_R}})^c \chi_{\tau_R} + Y_{23} \Phi_{BL} (\overline{\chi_{\mu_R}})^c \chi_{\tau_R} \end{aligned}$$

$$+Y_{33} \Phi_3 \overline{(\chi_{\tau_R})^c} \chi_{\tau_R} + \text{h.c.} \quad (4)$$

where

$$D_\mu \chi = \partial_\mu \chi + i g_{\text{BL}} Y_{\text{BL}}(Z_{\text{BL}})_\mu \chi.$$

The gauge coupling associated with $U(1)_{\text{B-L}}$ is g_{BL} and Z_{BL} is the corresponding gauge boson. The scalar potentials which are mentioned in the Lagrangian in Eq. 3 can be written as:

$$\begin{aligned} V^{\text{L}}(H, \xi, \Phi_3) = & -\mu_H^2 H^\dagger H + \lambda_H (H^\dagger H)^2 + M_\xi^2 \text{Tr}[\xi^\dagger \xi] + \lambda_\xi (\text{Tr}[\xi^\dagger \xi])^2 + \lambda'_\xi \text{Tr}[(\xi^\dagger \xi)^2] \\ & + \lambda_{\xi H} \text{Tr}[\xi^\dagger \xi] (H^\dagger H) + \lambda'_{\xi H} \left(H^\dagger \xi \xi^\dagger H \right) - \mu_{\Phi_3}^2 \Phi_3^\dagger \Phi_3 + \lambda_{\Phi_3} (\Phi_3^\dagger \Phi_3)^2 \\ & + \lambda_{H\Phi_3} (H^\dagger H) (\Phi_3^\dagger \Phi_3) + \lambda_{\xi\Phi_3} (\Phi_3^\dagger \Phi_3) \text{Tr}[\xi^\dagger \xi] \end{aligned} \quad (5)$$

$$\begin{aligned} V^{\text{H}}(\Delta, \Phi_{\text{BL}}, \Phi_{12}) = & M_\Delta^2 \text{Tr}[\Delta^\dagger \Delta] + \lambda_\Delta (\text{Tr}[\Delta^\dagger \Delta])^2 + \lambda'_\Delta \text{Tr}[(\Delta^\dagger \Delta)^2] \\ & - \mu_{\Phi_{\text{BL}}}^2 \Phi_{\text{BL}}^\dagger \Phi_{\text{BL}} + \lambda_{\Phi_{\text{BL}}} (\Phi_{\text{BL}}^\dagger \Phi_{\text{BL}})^2 + \lambda_{\Delta\Phi_{\text{BL}}} \text{Tr}[\Delta^\dagger \Delta] (\Phi_{\text{BL}}^\dagger \Phi_{\text{BL}}) \\ & - \mu_{\Phi_{12}}^2 \Phi_{12}^\dagger \Phi_{12} + \lambda_{\Phi_{12}} (\Phi_{12}^\dagger \Phi_{12})^2 + \lambda_{\Delta\Phi_{12}} \text{Tr}[\Delta^\dagger \Delta] (\Phi_{12}^\dagger \Phi_{12}) \\ & + \lambda_{\Phi_{\text{BL}}\Phi_{12}} (\Phi_{\text{BL}}^\dagger \Phi_{\text{BL}}) (\Phi_{12}^\dagger \Phi_{12}) + \lambda'_{\Phi_{\text{BL}}\Phi_{12}} (\Phi_{\text{BL}}^\dagger \Phi_{12}) (\Phi_{12}^\dagger \Phi_{\text{BL}}) \end{aligned} \quad (6)$$

$$\begin{aligned} V^{\text{LH}} = & \lambda_{\Delta H} \text{Tr}[\Delta^\dagger \Delta] (H^\dagger H) + \lambda'_{\Delta H} \left(H^\dagger \Delta \Delta^\dagger H \right) + [\mu_\Delta (H^T i \sigma^2 \Delta^\dagger H) + \text{h.c.}] \\ & + \lambda_{H\Phi_{\text{BL}}} (H^\dagger H) (\Phi_{\text{BL}}^\dagger \Phi_{\text{BL}}) + \lambda_{H\Phi_{12}} (H^\dagger H) (\Phi_{12}^\dagger \Phi_{12}) + \lambda_{\Phi_{\text{BL}}\Phi_3} (\Phi_{\text{BL}}^\dagger \Phi_{\text{BL}}) (\Phi_3^\dagger \Phi_3) \\ & + \lambda'_{\Phi_{\text{BL}}\Phi_3} (\Phi_{\text{BL}}^\dagger \Phi_3) (\Phi_3^\dagger \Phi_{\text{BL}}) + \lambda_{\Phi_{12}\Phi_3} (\Phi_{12}^\dagger \Phi_{12}) (\Phi_3^\dagger \Phi_3) + \lambda'_{\Phi_{12}\Phi_3} (\Phi_{12}^\dagger \Phi_3) (\Phi_3^\dagger \Phi_{12}) \\ & + \lambda_{\Delta\Phi_3} (\Delta^\dagger \Delta) (\Phi_3^\dagger \Phi_3) + \lambda_{\xi\Phi_{\text{BL}}} \text{Tr}[\xi^\dagger \xi] (\Phi_{\text{BL}}^\dagger \Phi_{\text{BL}}) + \lambda_{\xi\Phi_{12}} \text{Tr}[\xi^\dagger \xi] (\Phi_{12}^\dagger \Phi_{12}) \\ & + \lambda_{\Delta\xi} \text{Tr}[\Delta^\dagger \Delta] \text{Tr}[\xi^\dagger \xi] + \lambda'_{\Delta\xi} \text{Tr}[\Delta^\dagger \xi] \text{Tr}[\xi^\dagger \Delta] \\ & + \lambda_P \Phi_{\text{BL}}^2 \text{Tr}[\Delta^\dagger \xi] + \lambda_Q (\Phi_{\text{BL}}^\dagger)^2 \Phi_3 \Phi_{12} + \text{h.c.} \end{aligned} \quad (7)$$

Here it is worth mentioning that the mass squared terms of Δ and ξ are chosen to be positive so they do not get any spontaneous vev. Only the neutral components of $H, \Phi_{12}, \Phi_{\text{BL}}$ and Φ_3 acquire non-zero vevs. However, after electroweak phase transition, Δ and ξ acquire induced vevs.

For simplicity, we assume certain mass hierarchy among the scalars. The masses of H, Φ_3 and ξ are of similar order in sub-TeV range, while the masses of Φ_{BL} and Φ_{12} are in Several

TeV scale. To make the analysis simpler we decouple the light scalar sector from the heavy scalar sector by considering all quartic couplings in the scalar potential $V^{\mathbb{LH}}$ to be negligible. It is worth mentioning that this assumption does not affect our DM phenomenology.

We parameterize the neutral scalars in the low-energy scale as:

$$H^0 = \frac{v_H + h_H + i G_H}{\sqrt{2}} \quad , \quad \xi^0 = \frac{v_\xi + h_\xi + i G_\xi}{\sqrt{2}} \quad , \quad \Phi_3 = \frac{v_3 + h_3 + i G_{\Phi_3}}{\sqrt{2}} \quad .$$

A. NEUTRINO MASS

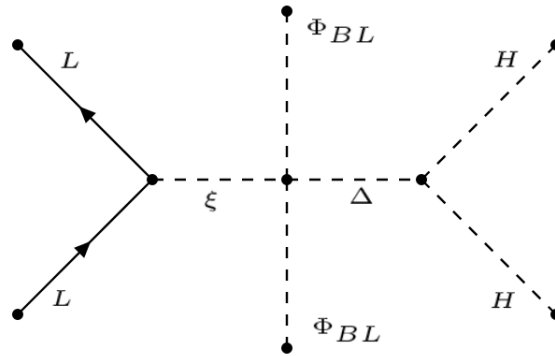


FIG. 1: Generation of neutrino mass through the modified Type-II seesaw.

The relevant Feynman diagram of this modified type-II seesaw which gives rise to light neutrino masses is as shown in Fig 1. In this modified version of type-II seesaw, the conventional heavy triplet scalar Δ can not generate Majorana masses for light neutrinos as the $B - L$ quantum number of Δ is zero. However this super heavy scalar Δ can mix with the TeV scalar triplet ξ , once Φ_{BL} acquires vev and breaks the $U(1)_{B-L}$ symmetry spontaneously. By the virtue of the trilinear term of Δ with SM Higgs doublet H , it gets an induced vev after electroweak symmetry breaking similar to the case of traditional type-II seesaw. The induced vev acquired by Δ after EW phase transition is given by

$$\langle \Delta \rangle = v_\Delta \simeq -\frac{\mu_\Delta v_H^2}{2\sqrt{2}M_\Delta^2} . \quad (8)$$

The vev of Δ is required to satisfy:

$$\rho \equiv \frac{M_W^2}{M_Z^2 \cos^2 \theta} = \frac{1 + 2x^2}{1 + 4x^2} \approx 1 \quad (9)$$

where $x = v_\Delta/v_H$. The above constraint implies that $|v_\Delta| \sim \mathcal{O}(1)$ GeV.

Since ξ mixes with Δ after $U(1)_{B-L}$ breaking, it also acquires an induced vev after EW symmetry breaking which is given by

$$\langle \xi \rangle = v_\xi = -\frac{\lambda_P v_{BL}^2}{4M_\xi^2} v_\Delta. \quad (10)$$

Assuming $\lambda_P v_{BL}^2 \sim M_\xi^2$, we obtain $v_\Delta \simeq v_\xi$, even if ξ and Δ have several orders of magnitude difference in their masses. After integrating out the heavy degrees of freedom in the Feynman diagram given in Fig. 1, we get the Majorana mass matrix of the light neutrinos to be

$$(M_\nu)_{ij} = Y_{ij}^\xi v_\xi = -Y_{ij}^\xi \frac{\lambda_P v_{BL}^2}{4M_\xi^2} v_\Delta. \quad (11)$$

As $v_\Delta \simeq v_\xi \sim \mathcal{O}(1)$ GeV, we obtain sub-eV neutrino masses. Here it is worth noticing that the mixing between the super heavy triplet scalar Δ and the TeV scale scalar triplet ξ gives rise to the neutrino mass. Essentially this set up can be thought of in an effective manner. After the $U(1)_{B-L}$ breaking, ξ develops an effective trilinear coupling with the SM Higgs *i.e.* $\mu_\xi \xi^\dagger H H$ where μ_ξ is given by $\mu_\xi = \mu_\Delta \langle \Phi_{BL} \rangle^2 / M_\Delta^2$. And this effective coupling is similar to the conventional type-II seesaw which leads to the generation of neutrino mass in this scenario.

B. SCALAR MASSES AND MIXING

As already discussed in the section II, the only significant mixing relevant for low energy phenomenological aspects is the mixing between H , ξ and Φ_3 since all other mixings are insignificant and can be neglected. In this section we only consider the light scalar sector, $V^\mathbb{L}(H, \xi, \Phi_3)$ which is relevant for low energy phenomenology.

The minimization conditions for the scalar potential are given by:

$$\begin{aligned} \mu_H^2 &= \frac{1}{2} \left(\lambda_{H\Phi_3} v_3^2 + 2\lambda_H v_H^2 + v_\xi^2 (\lambda_{\xi H} + \lambda'_{\xi H}) - 2\sqrt{2}\mu_\xi v_\xi \right) \\ M_\xi^2 &= \frac{1}{2} \left(-\lambda_{\xi\Phi_3} v_3^2 - v_H^2 (\lambda_{\xi H} + \lambda'_{\xi H}) + \frac{\sqrt{2}\mu_\xi v_H^2}{v_\xi} - 2v_\xi^2 (\lambda_\xi + \lambda'_\xi) \right) \\ \mu_{\Phi_3}^2 &= \frac{1}{2} (2\lambda_{\Phi_3} v_3^2 + \lambda_{H\Phi_3} v_H^2 + \lambda_{\xi\Phi_3} v_\xi^2) \end{aligned} \quad (12)$$

CP even scalar sector:

$$\begin{aligned}
\mathcal{L}_{\text{mass}} &= \frac{1}{2} \begin{pmatrix} h_H & h_\xi & h_3 \end{pmatrix} \begin{pmatrix} 2\lambda_H v_H^2 & v_H v_\xi (\lambda_{\xi H} + \lambda'_{\xi H}) & \lambda_{H\Phi_3} v_3 v_H \\ v_H v_\xi (\lambda_{\xi H} + \lambda'_{\xi H}) & \frac{\mu_\xi v_H^2}{\sqrt{2}v_\xi} + 2v_\xi^2 (\lambda_\xi + \lambda'_\xi) & \lambda_{\xi\Phi_3} v_3 v_\xi \\ \lambda_{H\Phi_3} v_3 v_H & \lambda_{\xi\Phi_3} v_3 v_\xi & 2\lambda_{\Phi_3} v_3^2 \end{pmatrix} \begin{pmatrix} h_H \\ h_\xi \\ h_3 \end{pmatrix} \\
&= \frac{1}{2} \begin{pmatrix} h_H & h_\xi & h_3 \end{pmatrix} \mathcal{M}^{\text{CP Even}} \begin{pmatrix} h_H \\ h_\xi \\ h_3 \end{pmatrix} \\
&= \frac{1}{2} \begin{pmatrix} H_1 & H_2 & H_3 \end{pmatrix} \left(\mathcal{O}^T \mathcal{M}^{\text{CP-Even}} \mathcal{O} \right) \begin{pmatrix} H_1 \\ H_2 \\ H_3 \end{pmatrix} \\
&= \frac{1}{2} \begin{pmatrix} H_1 & H_2 & H_3 \end{pmatrix} \begin{pmatrix} m_{H_1}^2 & 0 & 0 \\ 0 & m_{H_2}^2 & 0 \\ 0 & 0 & m_{H_3}^2 \end{pmatrix} \begin{pmatrix} H_1 \\ H_2 \\ H_3 \end{pmatrix} \tag{13}
\end{aligned}$$

Here \mathcal{O} is the orthogonal matrix which diagonalises the CP-even scalar mass matrix. Thus the flavor eigen states and the mass eigen states of these scalars are related by:

$$\begin{pmatrix} h_H \\ h_\xi \\ h_3 \end{pmatrix} = \begin{pmatrix} c_{12}c_{13} & c_{13}s_{12} & s_{13} \\ -c_{12}s_{13}s_{23} - c_{23}s_{12} & c_{12}c_{23} - s_{12}s_{13}s_{23} & c_{13}s_{23} \\ s_{12}s_{23} - c_{12}c_{23}s_{13} & -c_{12}s_{23} - c_{23}s_{12}s_{13} & c_{13}c_{23} \end{pmatrix} \begin{pmatrix} H_1 \\ H_2 \\ H_3 \end{pmatrix} \tag{14}$$

where we abbreviated $\cos \beta_{ij} = c_{ij}$ and $\sin \beta_{ij} = s_{ij}$, with $\{ij : 12, 13, 23\}$.

CP odd scalar:

Denoting the massive CP odd scalar state that emerges as A^0 , its mass is given by:

$$m_{A^0}^2 = \frac{\mu_\xi (v_H^2 + 4v_\xi^2)}{\sqrt{2}v_\xi} \tag{15}$$

Singly charged scalar:

The mass of the massive singly charged scalar state, H^\pm is given by:

$$m_{H^\pm}^2 = \frac{2\sqrt{2}\mu_\xi v_H^2 - \lambda'_{\xi H} v_H^2 v_\xi - 2\lambda'_{\xi H} v_\xi^3 + 4\sqrt{2}\mu_\xi v_\xi^2}{4v_\xi} \tag{16}$$

Doubly charged scalar:

The mass of the doubly charged scalar, $H^{\pm\pm}$ is given by:

$$m_{H^{\pm\pm}}^2 = -\frac{\lambda'_{\xi H} v_H^2}{2} + \frac{\mu_{\xi} v_H^2}{\sqrt{2} v_{\xi}} - \lambda'_{\xi} v_{\xi}^2 \quad (17)$$

$U(1)_{B-L}$ Gauge Boson mass: The Z_{BL} boson acquires mass through the vevs of Φ_{BL} , Φ_{12} , Φ_3 which are charged under $U(1)_{B-L}$ and is given by:

$$M_{Z_{BL}}^2 \simeq g_{BL}^2 (v_{BL}^2 + 64v_{12}^2 + 100v_3^2). \quad (18)$$

The quartic couplings of scalars are expressed in term of physical masses and are expressed as:

$$\begin{aligned} \lambda_H &= \frac{c_{13}^2 (c_{12}^2 m_{H_1}^2 + m_{H_2}^2 s_{12}^2) + m_{H_3}^2 s_{13}^2}{2v_H^2} \\ \lambda_{\xi H} &= \frac{c_{13}s_{13}s_{23} (-c_{12}^2 m_{H_1}^2 - m_{H_2}^2 s_{12}^2 + m_{H_3}^2) + c_{12}c_{13}c_{23}s_{12} (m_{H_2}^2 - m_{H_1}^2)}{v_H v_{\xi}} + \frac{4m_{H^{\pm}}^2}{v_H^2 + 2v_{\xi}^2} - \frac{2m_{A^0}^2}{v_H^2 + 4v_{\xi}^2} \\ \lambda_{\xi} &= \frac{s_{23}^2 (s_{13}^2 (c_{12}^2 m_{H_1}^2 + m_{H_2}^2 s_{12}^2) + c_{13}^2 m_{H_3}^2) + c_{23}^2 (c_{12}^2 m_{H_2}^2 + m_{H_1}^2 s_{12}^2) - 4m_{H^{\pm}}^2 + 2m_{H^{\pm\pm}}^2}{2v_{\xi}^2} \\ &\quad + \frac{2c_{12}c_{23}s_{12}s_{13}s_{23}(m_{H_1} - m_{H_2})(m_{H_1} + m_{H_2})}{2v_{\xi}^2} + \frac{4m_{H^{\pm}}^2}{v_H^2 + 2v_{\xi}^2} - \frac{2m_{A^0}^2}{v_H^2 + 4v_{\xi}^2} \\ \lambda'_{\xi} &= -\frac{m_{A^0}^2 - m_{H^{\pm\pm}}^2 - 2m_{H^{\pm}}^2}{v_{\xi}^2} + \frac{4m_{A^0}^2}{v_H^2 + 4v_{\xi}^2} - \frac{4m_{H^{\pm}}^2}{v_H^2 + 2v_{\xi}^2} \\ \lambda'_{\xi H} &= \frac{4m_{A^0}^2}{v_H^2 + 4v_{\xi}^2} - \frac{4m_{H^{\pm}}^2}{v_H^2 + 2v_{\xi}^2} \\ \lambda_{\Phi_3} &= \frac{m_{H_1}^2 (c_{12}c_{23}s_{13} - s_{12}s_{23})^2 + m_{H_2}^2 (c_{12}s_{23} + c_{23}s_{12}s_{13})^2 + c_{13}^2 c_{23}^2 m_{H_3}^2}{2v_3^2} \\ \lambda_{H\Phi_3} &= \frac{c_{13}c_{23}s_{13} (-c_{12}^2 m_{H_1}^2 - m_{H_2}^2 s_{12}^2 + m_{H_3}^2) + c_{12}c_{13}s_{12}s_{23}(m_{H_1} - m_{H_2})(m_{H_1} + m_{H_2})}{v_3 v_H} \\ \lambda_{\xi\Phi_3} &= \frac{m_{H_1}^2 (c_{12}s_{13}s_{23} + c_{23}s_{12})(c_{12}c_{23}s_{13} - s_{12}s_{23}) - m_{H_2}^2 (c_{12}s_{23} + c_{23}s_{12}s_{13})(c_{12}c_{23} - s_{12}s_{13}s_{23})}{v_3 v_{\xi}} \\ &\quad + \frac{c_{13}^2 c_{23} m_{H_3}^2 s_{23}}{v_3 v_{\xi}} \end{aligned} \quad (19)$$

Constraints on scalar sector:

Based on the measurement of the ρ parameter $\rho = 1.0008_{-0.0010}^{+0.0017}$ ([21, 46]), as discussed in Sec. II A, the triplet ξ vev can have an upper bound of order 2.5-4.6 GeV ([68]). Also the mixing angle between the SM Higgs and the triplet scalar is constrained from Higgs decay measurement. As obtained by [69], this mixing angle $\sin \beta_{12}$ is bounded above, in

particular, $\sin \beta_{12} \lesssim 0.05$ to be consistent with experimental observation of $H_1 \rightarrow WW^*$ [46, 69]. There are similar bounds on singlet scalar mixing with the SM Higgs boson. Such bounds come from both theoretical and experimental constraints [70, 71]. The upper bound on singlet scalar-SM Higgs mixing angle $\sin \beta_{13}$ comes from W boson mass correction [72] at NLO. For $250 \text{ GeV} < m_{H_3} < 850 \text{ GeV}$, $\sin \beta_{13}$ is constrained to be $\sin \beta_{13} < 0.2 - 0.3$ where m_{H_3} is the mass of the third physical Higgs.

For our further discussion we consider the following benchmark points where all the above mentioned constraints are satisfied:

$$\{m_{H_2} = 331.779, m_{H_3} = 366.784, m_{A^0} = 33, m_{H^\pm} = 369.841, m_{H^{\pm\pm}} = 404.343 \\ v_\xi = 2.951 \text{ (in GeV)}; s_{12} = 0.03, s_{23} = s_{13} = 0.01 \} \quad (20)$$

III. DARK MATTER

The $U(1)_{B-L}$ gauge symmetry gets spontaneously broken down by the vev of Φ_{12} , Φ_{B-L} and Φ_3 to a remnant \mathbb{Z}_2 symmetry under which the exotic fermions: χ_{i_R} ($i = e, \mu, \tau$) are assumed to be odd, while all other particles transforms trivially. As a result the lightest among these fermions becomes a viable candidate of DM and can give rise to the observed relic density by thermal freeze-out mechanism.

A. THE EXOTIC FERMIONS AND THEIR INTERACTIONS

From Eq. 3, the mass matrix for χ_{i_R} ($i = e, \mu, \tau$) in the effective theory can be written as:

$$-\mathcal{L}_\chi^{mass} = \frac{1}{2} \left(\overline{(\chi_{e_R})^c} \quad \overline{(\chi_{\mu_R})^c} \quad \overline{(\chi_{\tau_R})^c} \right) \mathcal{M} \begin{pmatrix} \chi_{e_R} \\ \chi_{\mu_R} \\ \chi_{\tau_R} \end{pmatrix} \quad (21)$$

where

$$\mathcal{M} = \frac{1}{\sqrt{2}} \begin{pmatrix} Y_{11}v_{12} & Y_{12}v_{12} & Y_{13}v_{BL} \\ Y_{12}v_{12} & Y_{22}v_{12} & Y_{23}v_{BL} \\ Y_{13}v_{BL} & Y_{23}v_{BL} & Y_{33}v_3 \end{pmatrix} = \begin{pmatrix} [M_{12}] & [M'] \\ [M']^T & M_3 \end{pmatrix}. \quad (22)$$

Here M_{12}, M', M_3 are:

$$M_{12} = \frac{1}{\sqrt{2}} \begin{pmatrix} Y_{11}v_{12} & Y_{12}v_{12} \\ Y_{12}v_{12} & Y_{22}v_{12} \end{pmatrix}, \quad M' = \frac{1}{\sqrt{2}} \begin{pmatrix} Y_{13}v_{\text{BL}} \\ Y_{23}v_{\text{BL}} \end{pmatrix}, \quad M_3 = \frac{1}{\sqrt{2}} (Y_{33}v_3).$$

For simplicity we assume $Y_{11} = Y_{22}$ and $Y_{13} = Y_{23}$. As a result the above Majorana fermion mass matrix \mathcal{M} can be exactly diagonalized by an orthogonal rotation $\mathcal{R} = \mathcal{R}_{13}(\theta) \cdot \mathcal{R}_{23}(\theta_{23} = 0) \cdot \mathcal{R}_{12}(\theta_{12} = \frac{\pi}{4})$ which is essentially characterized by only one parameter θ [73]. So we diagonalized the mass matrix \mathcal{M} as $\mathcal{R} \cdot \mathcal{M} \cdot \mathcal{R}^T = \mathcal{M}_{\text{Diag.}}$, where the \mathcal{R} is given by:

$$\mathcal{R} = \begin{pmatrix} \frac{1}{\sqrt{2}} \cos \theta & \frac{1}{\sqrt{2}} \cos \theta & \sin \theta \\ -\frac{1}{\sqrt{2}} & \frac{1}{\sqrt{2}} & 0 \\ -\frac{1}{\sqrt{2}} \sin \theta & -\frac{1}{\sqrt{2}} \sin \theta & \cos \theta \end{pmatrix} \quad (23)$$

Where the rotation parameter θ required for the diagonalization is given by:

$$\tan 2\theta = \frac{2\sqrt{2} Y_{13}v_{\text{BL}}}{(Y_{11} + Y_{12})v_{12} - Y_{33}v_3} \quad (24)$$

Thus the physical states of the exotic fermions are $\chi_i = \frac{\chi_{iR} + (\chi_{iR})^c}{\sqrt{2}}$ and are related to the flavor eigen states by the following linear combinations:

$$\begin{aligned} \chi_{1R} &= \frac{1}{\sqrt{2}} \cos \theta \chi_{eR} + \frac{1}{\sqrt{2}} \cos \theta \chi_{\mu R} + \sin \theta \chi_{\tau R} \\ \chi_{2R} &= -\frac{1}{\sqrt{2}} \chi_{eR} + \frac{1}{\sqrt{2}} \chi_{\mu R} \\ \chi_{3R} &= -\frac{1}{\sqrt{2}} \sin \theta \chi_{eR} - \frac{1}{\sqrt{2}} \sin \theta \chi_{\mu R} + \cos \theta \chi_{\tau R} \end{aligned} \quad (25)$$

And the corresponding mass eigen values are given by:

$$\begin{aligned} M_1 &= \frac{1}{2\sqrt{2}} \left[(Y_{11} + Y_{12})v_{12} + Y_{33}v_3 + \sqrt{((Y_{11} + Y_{12})v_{12} - Y_{33}v_3)^2 + 8(Y_{13}v_{\text{BL}})^2} \right] \\ M_2 &= \frac{1}{\sqrt{2}} (Y_{11} - Y_{12})v_{12} \\ M_3 &= \frac{1}{2\sqrt{2}} \left[(Y_{11} + Y_{12})v_{12} + Y_{33}v_3 - \sqrt{((Y_{11} + Y_{12})v_{12} - Y_{33}v_3)^2 + 8(Y_{13}v_{\text{BL}})^2} \right] \end{aligned} \quad (26)$$

Here it is worthy to mention that in the limit of $Y_{13} \rightarrow 0$ *i.e.* $\theta \rightarrow 0$, we get the mass eigen values of the DM particles as $M_{1,2} = \frac{1}{\sqrt{2}}(Y_{11} \pm Y_{12})v_{12}$ and $M_3 = \frac{1}{\sqrt{2}}Y_{33}v_3$ and the corresponding mass eigen states are $\chi_{1R,2R} = \frac{1}{\sqrt{2}}(\chi_{\mu R} \pm \chi_{eR})$ and $\chi_{3R} = \chi_{\tau R}$. If we assume that the off diagonal Yukawa coupling in M_{12} *i.e.* $Y_{12} \ll 1$, then χ_1 and χ_2 become almost degenerate.(*i.e.* $M_1 \simeq M_2$).

Assuming χ_3 to be the lightest state makes it the viable DM candidate and χ_1 and χ_2 are the next to lightest stable particles(NLSP). Using the relation $\mathcal{R}.\mathcal{M}.\mathcal{R}^T = \mathcal{M}_{Diag.}$, one can express the following relevant parameters in terms of the physical masses M_1, M_3 and the mixing angle $\sin \theta$ as

$$\begin{aligned} v_3 &= \frac{\sqrt{2}}{Y_{33}} (M_1 \sin^2 \theta + M_3 \cos^2 \theta) \\ v_{12} &= \frac{\sqrt{2}}{Y_{33} + Y_{12}} (M_1 \cos^2 \theta + M_3 \sin^2 \theta) \\ Y_{13} &= \frac{\Delta M \sin 2\theta}{2v_{BL}}. \end{aligned} \tag{27}$$

where ΔM is the mass splitting between the DM and NLSPs i.e. $\Delta M = M_1 - M_3$.

The gauge coupling g_{BL} can be expressed as

$$g_{BL} \simeq \frac{M_{Z_{BL}}}{\sqrt{(v_{BL}^2 + 64 v_{12}^2 + 100 v_3^2)}}. \tag{28}$$

The flavor eigen states can be expressed in terms of the physical eigen states as follows:

$$\begin{aligned} \chi_{e_R} &= \frac{1}{\sqrt{2}} \cos \theta \chi_{1_R} - \frac{1}{\sqrt{2}} \chi_{2_R} - \frac{1}{\sqrt{2}} \sin \theta \chi_{3_R} \\ \chi_{\mu_R} &= \frac{1}{\sqrt{2}} \cos \theta \chi_{1_R} + \frac{1}{\sqrt{2}} \chi_{2_R} - \frac{1}{\sqrt{2}} \sin \theta \chi_{3_R} \\ \chi_{\tau_R} &= \sin \theta \chi_{1_R} + \cos \theta \chi_{3_R} \end{aligned} \tag{29}$$

DM Interactions

The Yukawa and gauge interactions of DM relevant for the calculation of relic density can be written in the physical eigen states as follows:

$$\begin{aligned} \mathcal{L}_{Yuk.} &= Y_{33} \overline{(\chi_{\tau_R})^c} \chi_{\tau_R} \\ &= Y_{33} \left[(s_{12}s_{23} - c_{12}c_{23}s_{13})H_1 - (c_{12}s_{23} + c_{23}s_{12}s_{13})H_2 + (c_{13}c_{23})H_3 \right] \overline{(\chi_{\tau_R})^c} \chi_{\tau_R} \\ &= Y_{33} \left[(s_{12}s_{23} - c_{12}c_{23}s_{13})H_1 - (c_{12}s_{23} + c_{23}s_{12}s_{13})H_2 + (c_{13}c_{23})H_3 \right] \\ &\times \left[\sin^2 \theta \overline{(\chi_{1_R})^c} \chi_{1_R} + \cos^2 \theta \overline{(\chi_{3_R})^c} \chi_{3_R} + \sin \theta \cos \theta (\overline{(\chi_{1_R})^c} \chi_{3_R} + \overline{(\chi_{3_R})^c} \chi_{1_R}) \right] \end{aligned} \tag{30}$$

and

$$\begin{aligned}
\mathcal{L}_{Z_{\text{BL}}} = & g_{\text{BL}} \left[(4 \cos^2 \theta + 5 \sin^2 \theta) \overline{\chi_{1R}} \gamma^\mu \chi_{1R} + 4 \overline{\chi_{2R}} \gamma^\mu \chi_{2R} \right. \\
& \left. + (4 \sin^2 \theta + 5 \cos^2 \theta) \overline{\chi_{3R}} \gamma^\mu \chi_{3R} + \cos \theta \sin \theta (\overline{\chi_{1R}} \gamma^\mu \chi_{3R} + \overline{\chi_{3R}} \gamma^\mu \chi_{1R}) \right] (Z_{\text{BL}})_\mu
\end{aligned} \tag{31}$$

Note that there is no co-annihilation of χ_3 with χ_2 .

The dominant annihilation and co-annihilation channels for DM are shown in Fig 2-5 and Fig 6-9 respectively.

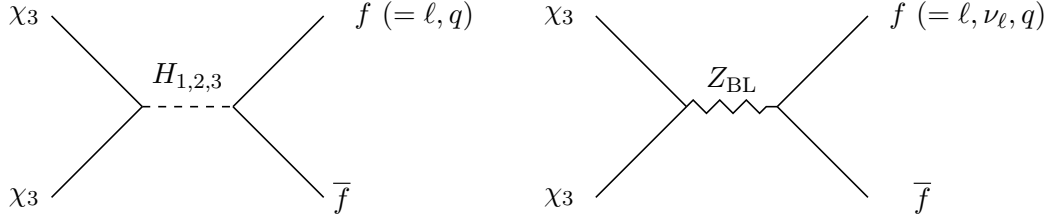


FIG. 2: Feynman diagrams for DM Annihilation: $\chi_3 \chi_3 \rightarrow f \bar{f}$.

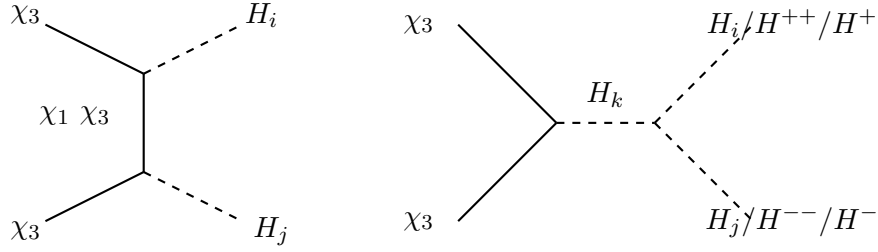


FIG. 3: Feynman diagrams for DM Annihilation: $\chi_3 \chi_3 \rightarrow H_i H_j$ ($i, j, k = 1, 2, 3$).

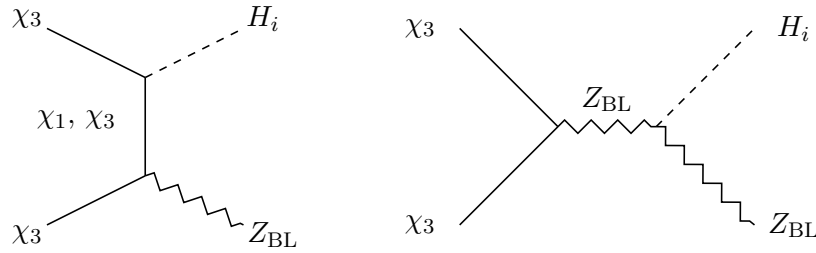


FIG. 4: Feynman diagrams for DM Annihilation: $\chi_3 \chi_3 \rightarrow H_i Z_{BL}$ ($i = 1, 2, 3$).

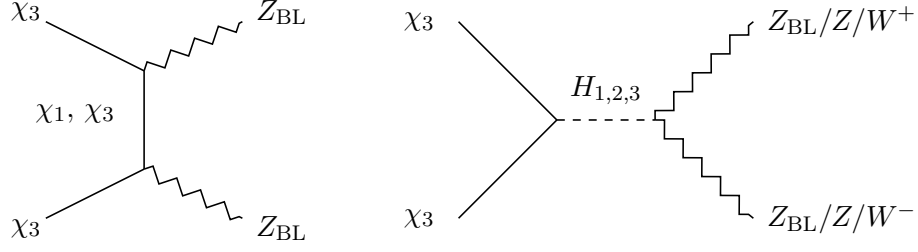


FIG. 5: Feynman diagrams for DM Annihilation: $\chi_3 \chi_3 \rightarrow Z_{BL} Z_{BL}; Z Z; W^+ W^-$.

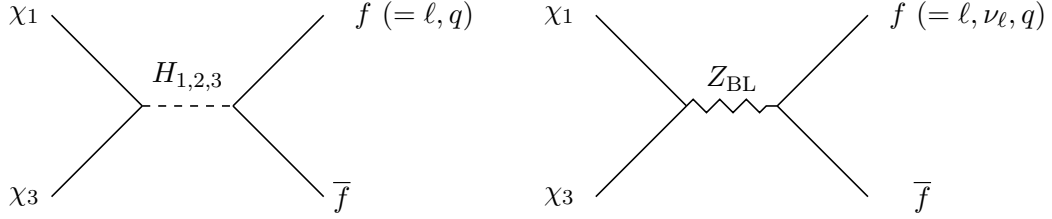


FIG. 6: Feynman diagrams for DM Co-Annihilation: $\chi_3 \chi_1 \rightarrow f \bar{f}$.

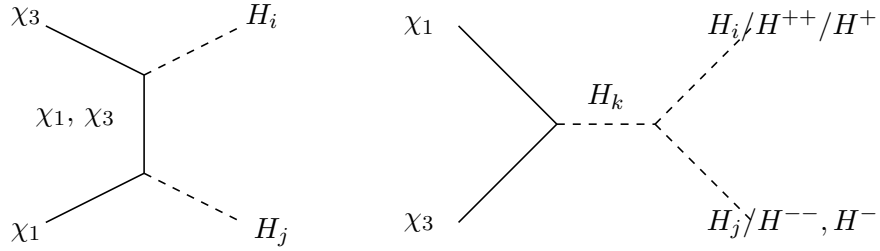


FIG. 7: Feynman diagrams for DM Co-Annihilation: $\chi_3 \chi_1 \rightarrow H_i H_j$ ($i, j, k = 1, 2, 3$).

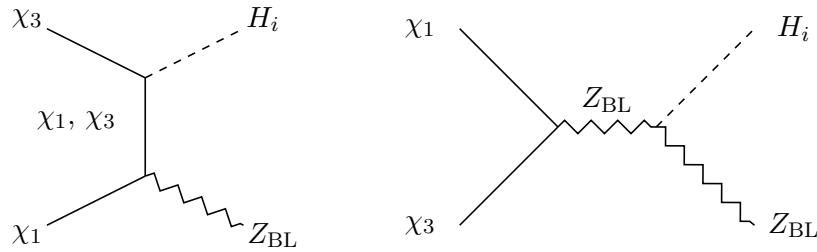


FIG. 8: Feynman diagrams for DM Co-Annihilation: $\chi_3 \chi_1 \rightarrow H_i Z_{BL}$ ($i = 1, 2, 3$).

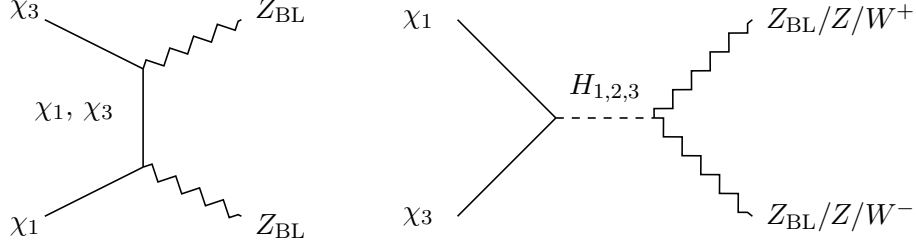


FIG. 9: Feynman diagrams for DM Co-Annihilation: $\chi_3 \chi_1 \rightarrow Z_{BL} Z_{BL}; Z Z; W^+ W^-$.

B. RELIC ABUNDANCE OF DM

The DM phenomenology is mainly governed by the following independent parameters:

$$\{ M_3 \equiv M_{DM}, \Delta M \equiv (M_1 - M_3) \simeq (M_2 - M_3), \sin \theta, Y_{33}, M_{Z_{BL}} \}. \quad (32)$$

while the other independent parameters that are kept fixed are: $v_{BL} = 10 \text{ TeV}$, $Y_{12} = 10^{-6}$, and the dependent parameters are g_{BL}, v_3, v_{12} and Y_{13} as mentioned in Eq 27,28.

The relic density of DM in this scenario can be estimated by solving the Boltzmann equation in the following form:

$$\frac{dn}{dt} + 3Hn = -\langle \sigma v \rangle_{eff} (n^2 - n_{eq}^2), \quad (33)$$

where n denotes number density of DM, i.e. $n \sim n_{\chi_3}$ and $n_{eq} = g(\frac{M_{DM}T}{2\pi})^{3/2} \exp(-M_{DM}/T)$ is equilibrium distribution. The DM freezes out giving us the thermal relic depending on $\langle \sigma v \rangle_{eff}$, which takes into account all number changing process listed in Fig 2-5 and Fig 6-9.

This can be written as:

$$\begin{aligned} \langle \sigma v \rangle_{eff} = & \frac{g_3^2}{g_{eff}^2} \langle \sigma v \rangle_{\chi_3 \chi_3} + \frac{2g_3 g_1}{g_{eff}^2} \langle \sigma v \rangle_{\chi_3 \chi_1} \left(1 + \frac{\Delta M}{M_{DM}} \right)^{\frac{3}{2}} \exp(-x \frac{\Delta M}{M_{DM}}) \\ & + \frac{g_1^2}{g_{eff}^2} \langle \sigma v \rangle_{\chi_1 \chi_1} \left(1 + \frac{\Delta M}{M_{DM}} \right)^3 \exp(-2x \frac{\Delta M}{M_{DM}}) + \frac{g_2^2}{g_{eff}^2} \langle \sigma v \rangle_{\chi_2 \chi_2} \left(1 + \frac{\Delta M}{M_{DM}} \right)^3 \exp(-2x \frac{\Delta M}{M_{DM}}) \end{aligned} \quad (34)$$

Writing this equation in a precise form for convenience in discussion:

$$\begin{aligned} \langle \sigma v \rangle_{eff} = & \frac{g_3^2}{g_{eff}^2} \langle \sigma v \rangle_{\chi_3 \chi_3} + \langle \sigma v \rangle_{\chi_3 \chi_1} f(\Delta M, M_{DM}) \\ & + \langle \sigma v \rangle_{\chi_1 \chi_1} h_1(\Delta M, M_{DM}) + \langle \sigma v \rangle_{\chi_2 \chi_2} h_2(\Delta M, M_{DM}) \end{aligned} \quad (35)$$

where f, h_1 and h_2 are the factors multiplied to the co-annihilation cross-sections which are functions of ΔM .

Here g_{eff} is the effective degrees of freedom which can be expressed as,

$$g_{eff} = g_3 + g_1 \left(1 + \frac{\Delta M}{M_{DM}}\right)^{\frac{3}{2}} \exp\left(-x \frac{\Delta M}{M_{DM}}\right) + g_2 \left(1 + \frac{\Delta M}{M_{DM}}\right)^{\frac{3}{2}} \exp\left(-x \frac{\Delta M}{M_{DM}}\right) \quad (36)$$

where g_3 , g_1 , g_2 are the internal degrees of freedom of χ_3 , χ_1 and χ_2 respectively. The dimensionless parameter x is defined as $x = \frac{M_{DM}}{T} = \frac{M_3}{T}$.

The relic density of the DM (χ_3) then can be given by [74–76]:

$$\Omega_{\chi_3} h^2 = \frac{1.09 \times 10^9 \text{GeV}^{-1}}{g_*^{1/2} M_{Pl}} \frac{1}{J(x_f)} \quad (37)$$

where $g_* = 106.7$ and $J(x_f)$ is given by

$$J(x_f) = \int_{x_f}^{\infty} \frac{\langle \sigma v \rangle_{eff}}{x^2} dx \quad (38)$$

Here $x_f = \frac{M_{DM}}{T_f}$, and T_f denotes the freeze-out temperature of the DM χ_3 . We may note here that for correct relic $x_f \simeq 25$.

It is worth mentioning here that we used the package **MicrOmegas** [77] for computing annihilation cross-section and relic density, after generating the model files using **LanHEP** [78].

1. PARAMETER SPACE SCAN

To understand the DM relic density and the specific role of the model parameters in giving rise to the observed relic density, we performed several analysis and scan for allowed parameter space. As discussed in section III A, the important relevant parameters controlling the relic abundance of DM are: the mass of DM (M_{DM}), mass splitting(ΔM) between the DM (χ_3) and the next to lightest stable particle (χ_2 and χ_1 as $M_1 \simeq M_2$), and the mixing angle $\sin \theta$. Apart from these three, another crucial parameter which has a noteworthy effect on DM relic as well as other phenomenological aspects is the Yukawa coupling Y_{33} . We also keep the B – L gauge boson mass ($M_{Z_{BL}}$) as a free parameter. The dependent parameters have already been mentioned in Eqs. 27 and 28. The other parameters that are kept fixed judiciously during the analysis are $v_{BL} = 10 \text{ TeV}$ and $Y_{12} = 10^{-6}$.

We show the variation of relic density of DM χ_3 in Fig. 10 as a function of its mass M_{DM} for different choices of ΔM : 1-10 GeV, 20-50 GeV and 100-200 GeV shown by different colored points as mentioned in the inset of the figure. The dips in the relic density plots are essentially due to resonances corresponding to SM-Higgs, second Higgs and Z_{BL} gauge bosons

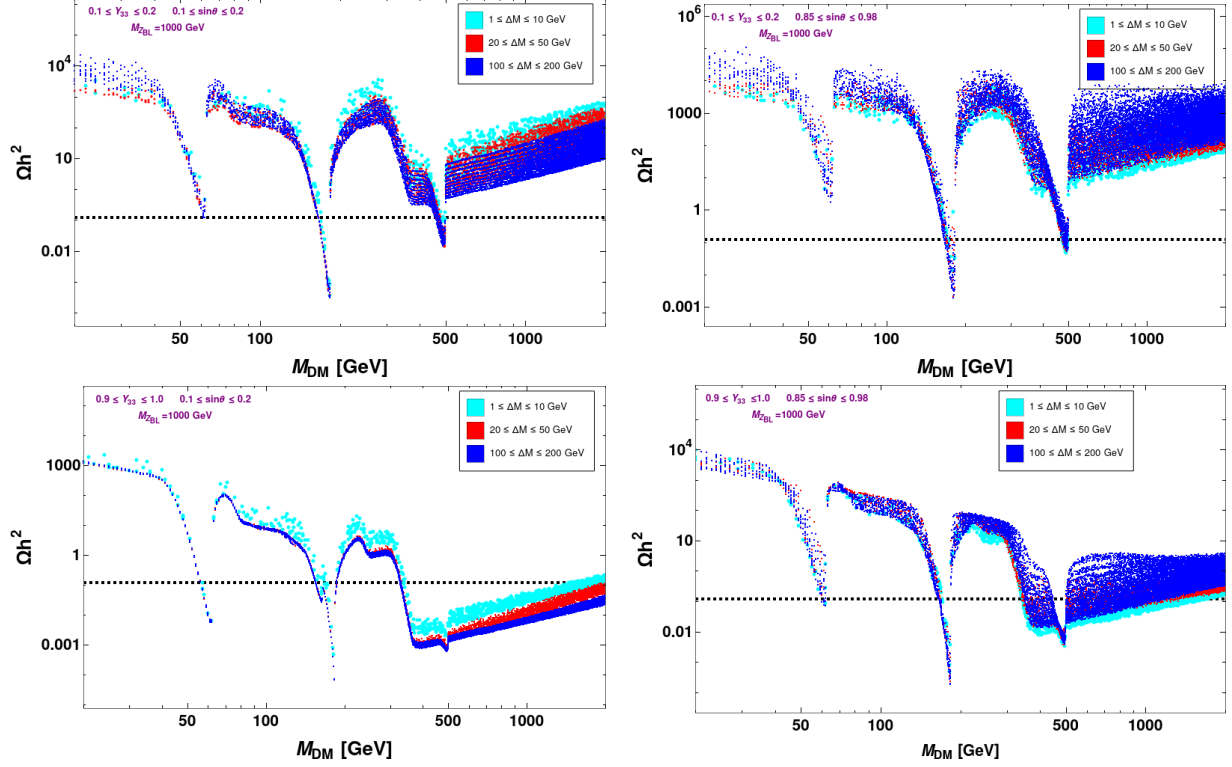


FIG. 10: Variation of relic density as a function of DM mass. Other parameters are kept fixed as mentioned inset of each figure .

respectively. In the top-left and top-right panel, Y_{33} is varied in a range $0.1 \leq Y_{33} \leq 0.2$ where as in the bottom-left and bottom-right panel it is varied in an interval $0.9 \leq Y_{33} \leq 1$. Clearly as Y_{33} increases, the effective annihilation cross-section increases which decreases the relic density. For a properly chosen value of Y_{33} (with other parameters fixed), we can obtain the correct relic density for a wide range of DM mass (M_{DM}).

We can also analyze the effect of mixing angle $\sin \theta$ and mass splitting (ΔM) from the results in Fig 10. Here it is worth mentioning that the parameter which decides the contribution of co-annihilations of DM to the relic density is $\sin \theta$ which can be understood by looking at Eq. 30 and 31. If $\sin \theta$ is small then contribution from annihilation of DM will dominate over all co-annihilation effects but for larger $\sin \theta$, co-annihilation contributions will be more as compared to the annihilations. The value of $\sin \theta$ predominantly decides the relative contribution of annihilation and co-annihilations of DM for the calculation of relic density. However the mass-splitting also plays a crucial role in the effect of annihilations and co-annihilations of DM. In the top and bottom right panel of Fig 10, $\sin \theta$ is randomly varied

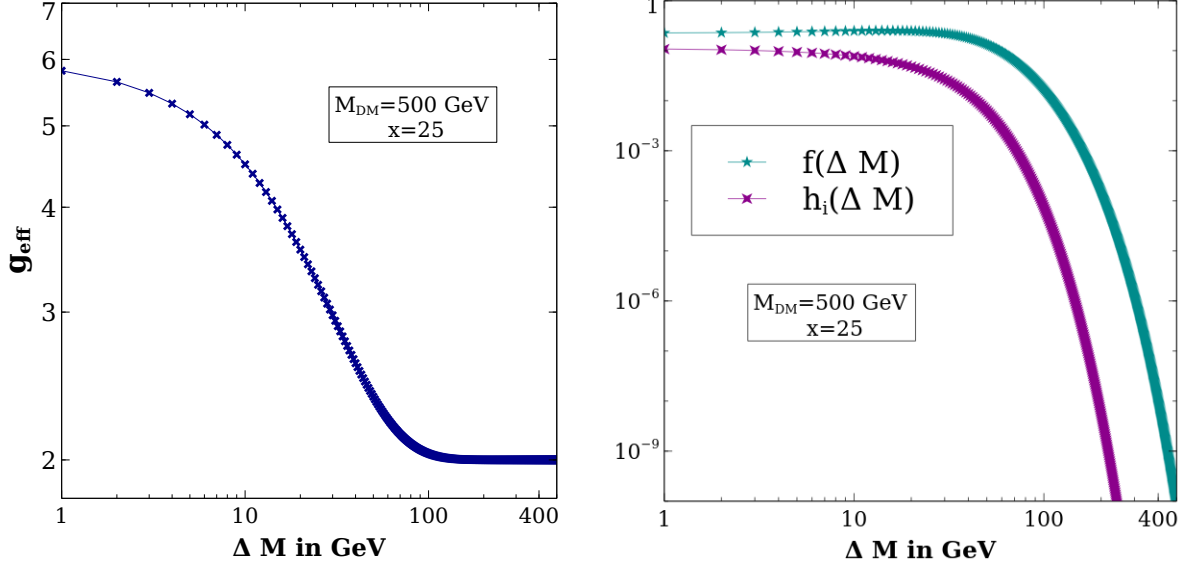


FIG. 11: [Left]: Variation of g_{eff} with ΔM , [Right]: Variation of $f(\Delta M) = \frac{2g_3g_1}{g_{\text{eff}}^2} \left(1 + \frac{\Delta M}{M_{\text{DM}}}\right)^{\frac{3}{2}} \exp\left(-x \frac{\Delta M}{M_{\text{DM}}}\right)$ and $h_{1,2}(\Delta M) = \frac{g_{1,2}^2}{g_{\text{eff}}^2} \left(1 + \frac{\Delta M}{M_{\text{DM}}}\right)^3 \exp\left(-2x \frac{\Delta M}{M_{\text{DM}}}\right)$ with ΔM .

in a range $0.85 \leq \sin \theta \leq 0.98$ for two different ranges of Y_{33} . For such a large $\sin \theta$, DM annihilates very weakly, so the co-annihilations essentially decides the effective annihilation cross-section and hence the relic density. This means in Eq. 34, the first term is negligible as compared to the other terms. In such a case, as ΔM increases, these co-annihilations become less and less effective thus decreasing the effective annihilation cross-section hence increasing the relic density. This trend is clearly observed in the right panel plots of Fig 10. The effect of mass splitting in such a case can also be understood by looking at the right panel of Fig 11 where the multiplying functions (mentioned as $f(\Delta M)$ and $h(\Delta M)$) in the co-annihilation terms of the effective annihilation cross-section in Eq. 35, are plotted as a function of mass-splitting ΔM . As ΔM increases, these factors decrease drastically consequently decreasing the overall effective annihilation cross-section and hence increasing the relic density of DM.

However if we consider the case of smaller $\sin \theta$ as considered for the left panel plots of Fig 10 (*i.e.* $0.1 \leq \sin \theta \leq 0.2$), here DM annihilation is the most effective and hence dominantly decides the relic density and except the first term in Eq. 34, other terms are negligible. In this case, with increase in mass splitting the effective thermal averaged cross-section increases and relic density decreases. This is due to the fact that, when ΔM increases,

the effective degrees of freedom g_{eff} decreases which is shown in the left panel plot of Fig 11 for a benchmark value of M_{DM} . This in turn increases the $\langle\sigma v\rangle_{eff}$ and hence results in decrease in the DM relic abundance.

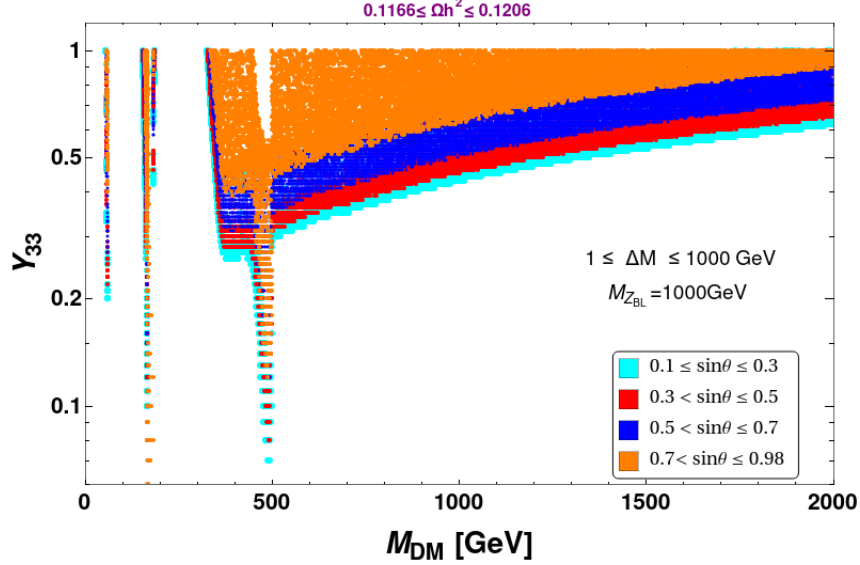


FIG. 12: Relic density allowed parameters space in $M_{DM} - Y_{33}$ plane for different intervals of $\sin \theta_{13}$.

To make the analysis more robust, in Fig. 12, the correct relic density allowed parameter space has been shown in the plane of Y_{33} vs M_{DM} for wide range of mixing angle $\{\sin \theta = 0.1 - 0.3, 0.3 - 0.5, 0.5 - 0.7, 0.7 - 0.98\}$, indicated by different colors. To carry out this scan of parameter space, ΔM is varied randomly within 1 to 1000 GeV. We can see that at the resonance regions, any value of Y_{33} can give rise to correct relic abundance. However for other values of M_{DM} , a relatively larger Y_{33} is required to obtain the correct relic.

In Fig 13, a scan similar to Fig 12 is carried out for correct relic density allowed parameter space in the M_{DM} vs Y_{33} plane, with ΔM varied randomly in different intervals for 3 different range of $\sin \theta$.

From this analysis, the riveting feature of this model that comes out is that, as compared to the earlier $U(1)_{B-L}$ models with right handed neutrino (RHN) dark matter where the correct relic density is usually achieved for DM mass near the resonance (i.e. $M_{DM} \sim M_{Z_{BL}}/2$) [56, 60–62], the crucial difference here is; in addition to the resonances, we obtain a large parameter space satisfying correct relic density for larger Yukawa coupling Y_{33} due to co-annihilations among the dark sector particles.

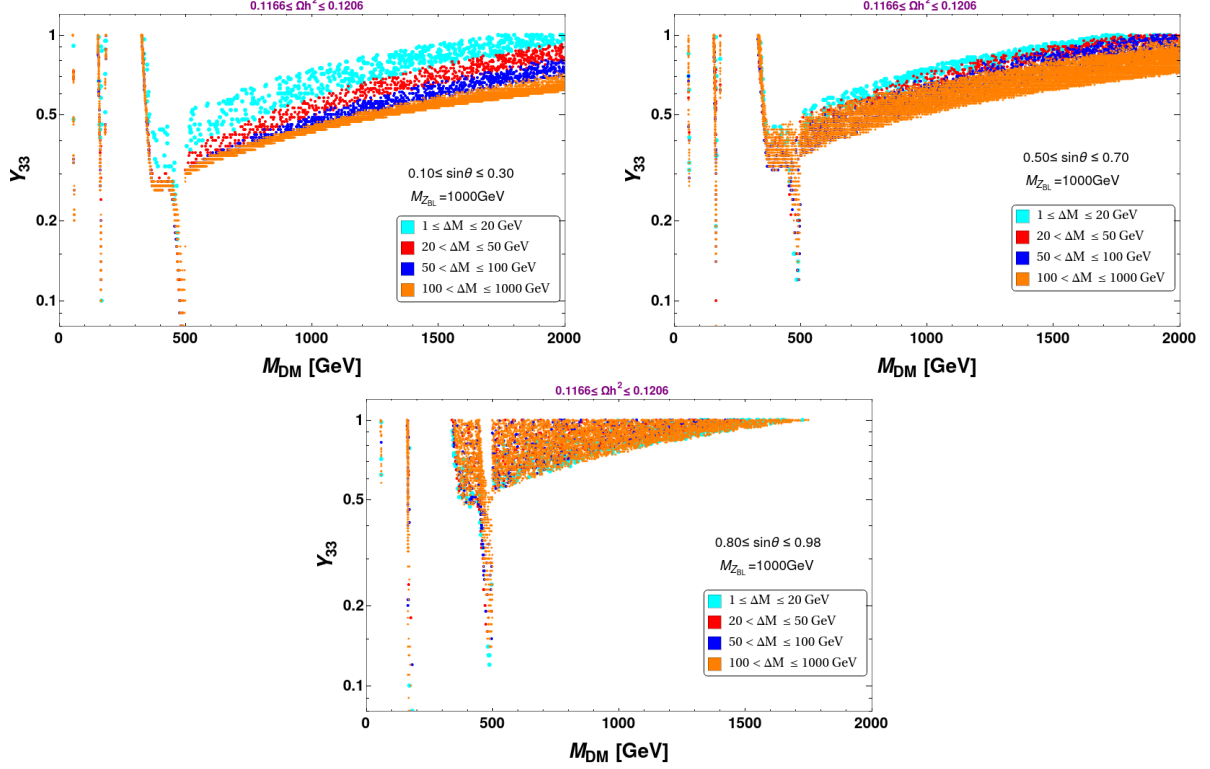


FIG. 13: Relic density allowed parameters space in $M_{DM} - Y_{33}$ plane for different ΔM as specified in the figure inset.

IV. DETECTION PROSPECTS OF DM

A. DIRECT DETECTION

There are various attempts to detect DM. One such major experimental procedure is the Direct detection of the DM at terrestrial laboratories through elastic scattering of the DM off nuclei. Several experiments put strict bounds on the dark matter nucleon cross section like LUX [9], PandaX-II [10, 11] and XENON-1T [12, 13]. In this model, the DM-nucleon scattering is possible via Higgs-mediated interaction represented by the Feynman diagram shown in Fig 14. Here, it is worth mentioning that the DM being a Majorana fermion has only the off diagonal (axial vector) couplings with the Z_{BL} boson and therefore do not contribute to spin independent direct search.

The cross section per nucleon for the spin-independent (SI) DM-nucleon interaction is given by:

$$\sigma_{SI} = \frac{1}{\pi A^2} \mu_r^2 |\mathcal{M}|^2, \quad (39)$$

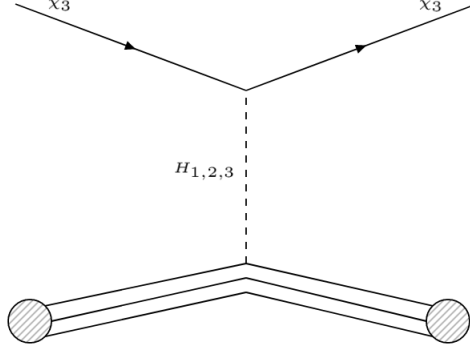


FIG. 14: Higgs-mediated DM-nucleon scattering

where A is the mass number of the target nucleus, μ_r is the reduced mass of the DM-nucleon system and \mathcal{M} is the amplitude for the DM-nucleon interaction, which can be written as:

$$\mathcal{M} = [Zf_p + (A - Z)f_n], \quad (40)$$

where f_p and f_n denote effective interaction strengths of DM with proton and neutron of the target used with A being mass number and Z being atomic number. The effective interaction strength can then further be decomposed in terms of interaction with partons as:

$$f_{p,n}^i = \sum_{q=u,d,s} f_{T_q}^{p,n} \alpha_q^i \frac{m_{p,n}}{m_q} + \frac{2}{27} f_{T_G}^{p,n} \sum_{Q=c,t,b} \alpha_Q^i \frac{m_{p,n}}{m_Q}, \quad (41)$$

with

$$\begin{aligned} \alpha_q^1 &= -Y_{33} \cos^2 \theta \frac{m_q}{v_H} \left[\frac{(s_{12}s_{23} - c_{12}c_{23}s_{13})^2}{m_{H_1}^2} \right] \\ \alpha_q^2 &= -Y_{33} \cos^2 \theta \frac{m_q}{v_H} \left[\frac{(c_{12}s_{23} + c_{23}s_{12}s_{13})^2}{m_{H_2}^2} \right] \\ \alpha_q^3 &= -Y_{33} \cos^2 \theta \frac{m_q}{v_H} \left[\frac{(c_{13}c_{23})^2}{m_{H_3}^2} \right] \end{aligned} \quad (42)$$

coming from DM interaction with SM via Higgs portal coupling. In Eq.41, the different coupling strengths between DM and light quarks are given in ref. [1, 79] as $f_{T_u}^p = 0.020 \pm 0.004$, $f_{T_d}^p = 0.026 \pm 0.005$, $f_{T_s}^p = 0.014 \pm 0.062$, $f_{T_u}^n = 0.020 \pm 0.004$, $f_{T_d}^n = 0.036 \pm 0.005$, $f_{T_s}^n = 0.118 \pm 0.062$. The coupling of DM with the gluons in target nuclei is parameterized by:

$$f_{T_G}^{(p,n)} = 1 - \sum_{q=u,d,s} f_{T_q}^{p,n}.$$

In the context of DM direct search, the model parameters that enter the DM-nucleon direct search cross-section, are the Higgs-DM Yukawa coupling (Y_{33}) and the mixing angle ($\sin \theta$), which can be constrained by requiring that σ_{SI} is less than the current DM-nucleon cross-sections dictated by non-observation of DM in current direct search data. In Fig. 15, we show the DM-nucleon cross section mediated by scalars in comparison to the latest XENON1T bound. In left panel of Fig. 15, we confronted the points satisfying relic density with the spin independent DM-nucleon elastic scattering cross section obtained for the model as a function of DM mass. The XENON1T bound is shown by dashed black line. Thus the region below this line satisfy both relic density as well as direct detection constraint. We can see that, though for DM mass at the resonance regions, $\sin \theta$ values $0.1 - 0.98$ can satisfy the direct detection constraint but for DM masses other than at the resonances, only larger $\sin \theta$ values ($0.7 \leq \sin \theta \leq 0.98$) are favored which is indicated by the orange points. As we have already discussed that in the larger $\sin \theta$ regime, the relic density is governed predominantly through the co-annihilations of DM, so this result interestingly implies that the co-annihilation effect essentially enhances the parameter space that satisfies the direct search constraints other than the resonance regions.

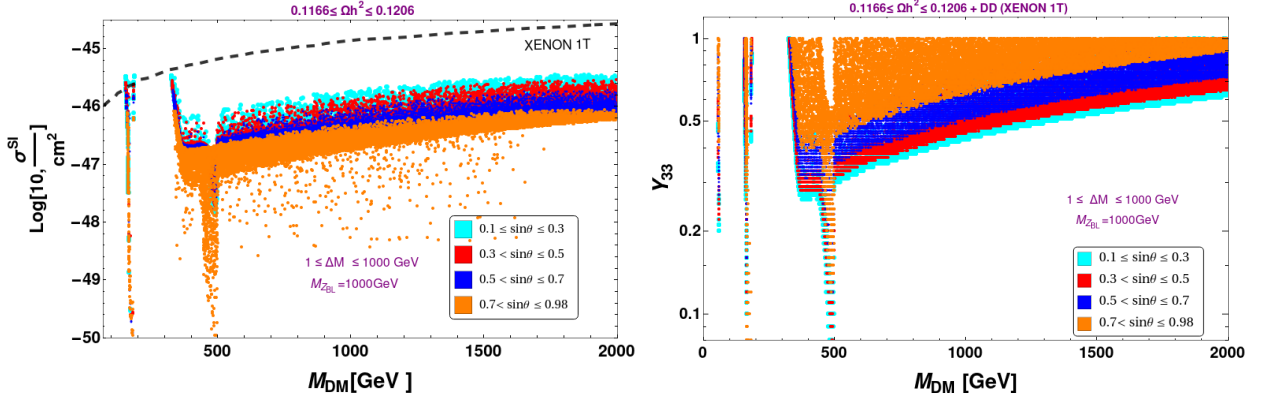


FIG. 15: [Left]: Spin-independent direct detection cross section of DM with nucleon as a function of DM mass (in GeV) confronted with XENON-1T data over and above relic density constraint from PLANCK. [Right]: Points satisfying both relic density constraint and Direct Detection constraint are projected in the $Y_{33} - M_{DM}$ plane. Different colors depict the different range of values of $\sin \theta$ as mentioned in the figure inset.

We again show the points satisfying relic density as well as direct detection constraint from XENON-1T in the plane of Y_{33} vs M_{DM} in the right panel of Fig. 15. Except for the

resonances, where all values of Y_{33} (*i.e.* $0.1 - 0.98$), satisfies both relic and DD constraints, for other values of DM mass, only with larger Y_{33} ; $0.6 \leq Y_{33} \leq 1$ these constraints can be satisfied. This plot again reinforces the fact that, though for DM mass near the resonances, all $\sin \theta$ values $0.1 - 0.98$ are allowed by the direct detection constraint but for DM mass other than at the resonances, only larger $\sin \theta$ values ($0.7 \leq \sin \theta \leq 0.98$) are favored.

B. INDIRECT DETECTION

Apart from direct detection experiments, DM can also be probed at different indirect detection experiments which essentially search for SM particles produced through DM annihilations. Among these final states, photon and neutrinos, being neutral and stable can reach the indirect detection experiments without getting affected much by intermediate medium between the source and the detector. For DM in the WIMP paradigm, these photons lie in the gamma ray regime and hence can be measured at space based telescopes like the Fermi Large Area Telescope (FermiLAT) or ground based telescopes like MAGIC. Measuring the gamma ray flux and using the standard astrophysical inputs, one can constrain the DM annihilation into different final states like $\mu^+\mu^-$, $\tau^+\tau^-$, W^+W^- , $b\bar{b}$. Since DM can not couple to photons directly, gamma rays can be produced from such charged final states. Using the bounds on DM annihilation to these final states from the indirect detection bounds arising from the global analysis of the Fermi-LAT and MAGIC observations of dSphs [14, 15], we check for the constraints on our DM parameters. Since there are multiple annihilation channels to different final states, the Fermi-LAT constraints on individual final states are weak for most of the cases. In Fig. 16(Left panel), we show the points satisfying both relic constraint and direct search constraint confronted with the constraints from indirect detection from MAGIC+FermiLAT for annihilation of DM to $W^+ W^-$ which is the most stringent as compared to DM annihilation to other channels. The combined bound from MAGIC and FermiLAT is shown by the black dotted line. The points below this line are allowed by relic, direct and indirect search constraints. In the right panel of Fig. 16, we represent the parameter space allowed by relic, direct as well as indirect search constraints in the plane of Y_{33} vs M_{DM} . Here also we see that the parameter space that satisfies relic and direct detection governed through the co-annihilation effects, are also consistent with the constraints from indirect search of DM.

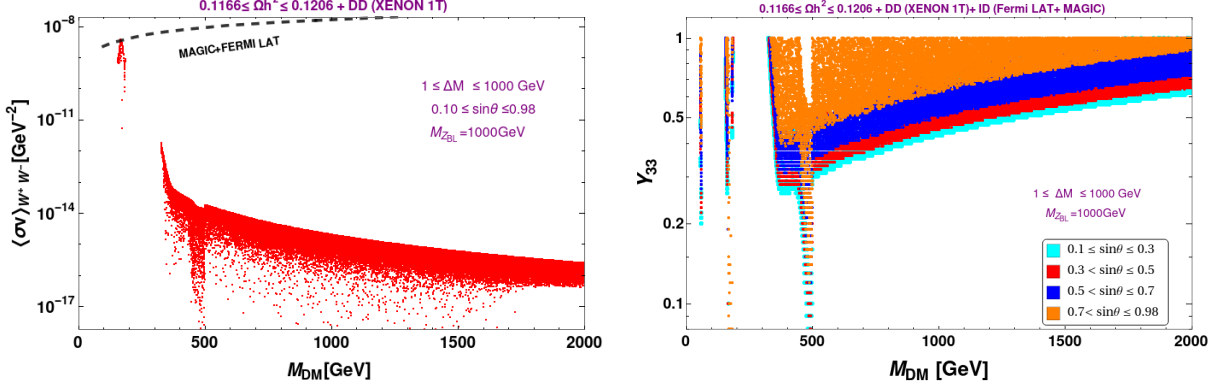


FIG. 16: [Left] $\langle\sigma v\rangle_{\chi_3\chi_3 \rightarrow W^+W^-}$ is shown as a function of M_{DM} . Only the points satisfying both Relic and DD constraints are shown. [Right] Relic+DD+ID allowed parameters are plotted in $M_{DM} - Y_{33}$ plane. Other parameters are kept fixed as mentioned in the inset of each figure

C. COLLIDER CONSTRAINTS ON $g_{BL} - M_{Z_{BL}}$

Apart from constraints from relic density and direct, indirect search of DM, there exists stringent experimental constraints on the B–L gauge sector from colliders like ATLAS, CMS and LEP-II. There exists a lower bound on the ratio of new gauge boson mass to the new gauge coupling $M_{Z'}/g' \geq 7$ TeV from LEP-II data [80, 81]. However the bounds from the current LHC experiments have already surpassed the LEP II limits. In particular, search for high mass Di-lepton resonances have put strict bounds on such additional gauge sector. The latest bounds from the ATLAS experiment [82, 83] and the CMS experiment [84] at the LHC rule out such gauge boson masses below 4.3 TeV for g_{BL} of the same order as that of SM coupling, from analysis of 13 TeV data. However such bounds get weaker, if the corresponding gauge couplings are smaller [82] than the electroweak gauge couplings.

In Fig. 17, we show a parameter scan in the plane of g_{BL} vs M_{DM} to scrutinize our parameter space with respect to the constraints from ATLAS and LEP-II. The bounds on g_{BL} for a fixed $M_{Z_{BL}} (= 1000$ GeV) from both LEP-II and ATLAS are shown by dotted black lines. It is clear that the constraint from LEP-II is much weaker than the constraints from ATLAS. Only those points which lie below this black dotted line is allowed from all the relevant constraints (*i.e.* Relic + Direct Detection + Indirect Detection + ATLAS). The different colored points depict different Y_{33} values. From this analysis, as it is clear from Fig. 17, it can be inferred that all the relevant constraints as discussed above are getting

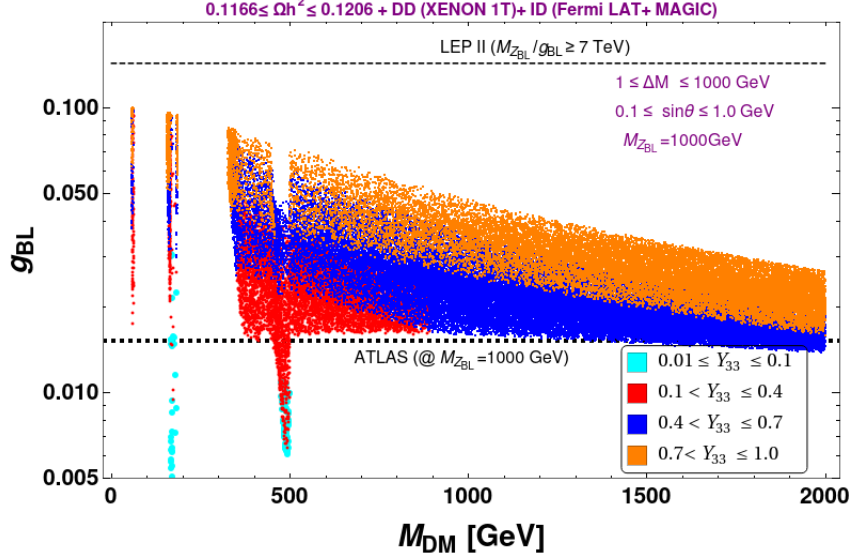


FIG. 17: g_{BL} vs M_{DM} plot. ATLAS and LEP-II bounds are shown for $M_{Z_{B-L}} = 1$ TeV.

satisfied at the resonance regions. However, some of the points corresponding to larger Y_{33} values beyond 0.4 are also allowed from all these constraints for M_{DM} beyond 1 TeV.

1 GeV $\leq M_{Z_{BL}} \leq 4000$ GeV:

So far whatever analysis we have done is with a fixed mass of the B – L gauge boson $M_{Z_{BL}} = 1000$ GeV. But if we vary the mass of Z_{BL} boson in a range $1 \text{ GeV} \leq M_{Z_{BL}} \leq 4000$ GeV, then the parameter space is shown in Fig. 18. This figure is similar to the Fig. 15, the only difference being the variation of $M_{Z_{BL}}$ in the later one. All the points below the black dotted line, are allowed by the relic as well as the direct detection constraint. On the right panel of Fig. 18, the parameter space consistent with all the constraints except from colliders(ATLAS) is shown in the plane of Y_{33} vs M_{DM} . Different colors are used to specify the value of $\sin \theta$ in different intervals during the scan.

We now turn to find the allowed parameter space in light of ATLAS bound on $g_{BL} - M_{Z_{BL}}$. The constraint on g_{BL} for corresponding values of $M_{Z_{BL}}$ coming from the non-observation of a new gauge boson (Z_{BL}) at LHC from ATLAS [82] analysis is shown by the black thick dotted line in right panel of Fig. 19. This indicates that points below the line with smaller g_{BL} is allowed, while those above the line are ruled out. The plot shows points which satisfy relic density constraint, direct as well as indirect search constraints. Different colors indicate

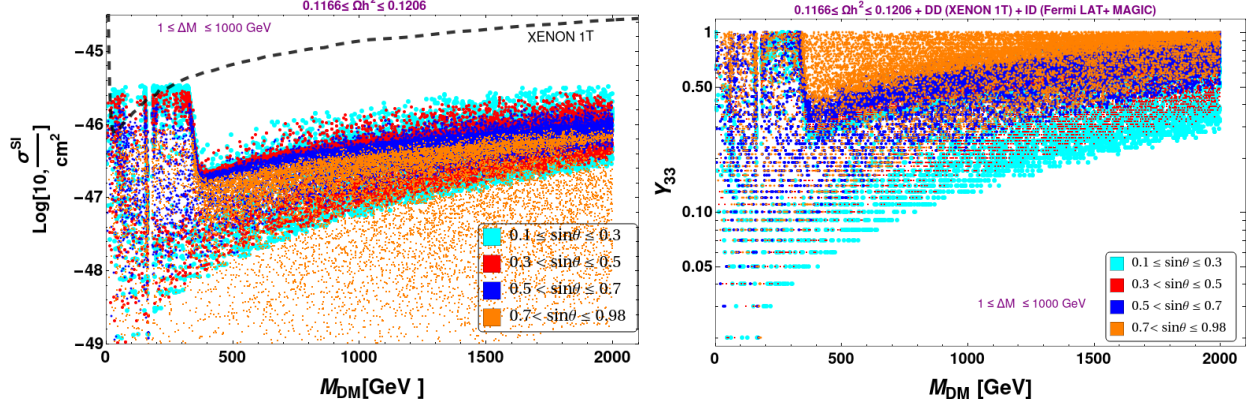


FIG. 18: [Left]: Spin-independent direct detection cross section of DM with nucleon as a function of DM mass (in GeV) confronted with XENON-1T data with M_{ZBL} varied in a range of 1 GeV to 4000 GeV. All points are satisfied the relic density constraint from PLANCK. [Right]: Points satisfying all these constraints (Relic+ Direct Detection+ Indirect Detection) projected in the Y_{33} vs M_{DM} plane.

ranges of Y_{33} as mentioned in figure inset.

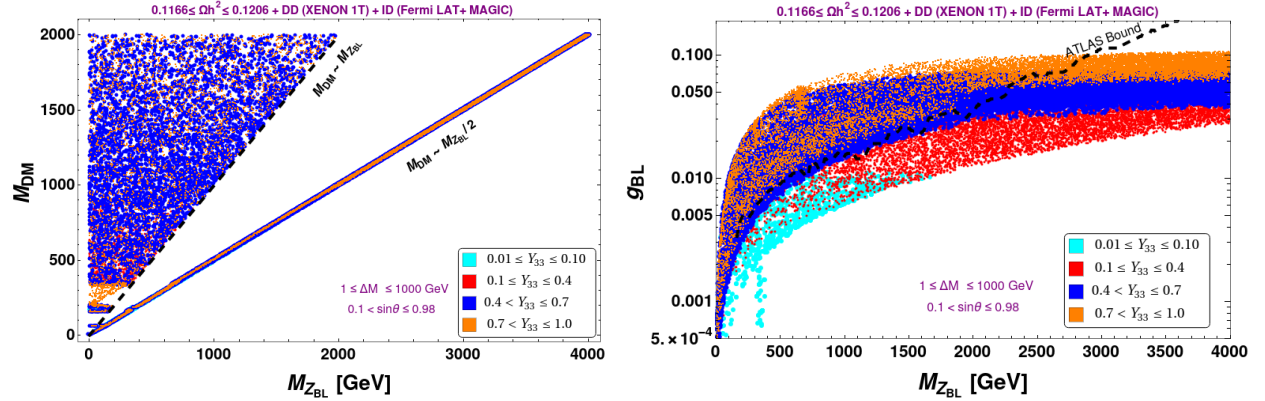


FIG. 19: Relic, direct detection and indirect detection satisfied points are shown in $M_{DM} - M_{ZBL}$ plane in left figure and $g_{BL} - M_{ZBL}$ plane in right figure with different range of Y_{33} . The thick black dotted line in right panel figure shows the ATLAS bound on g_{BL} vs M_{ZBL} plane from non-observation of Z_{BL} at colliders.

We then showcase the final parameter space in the plane of M_{DM} vs M_{ZBL} and Y_{33} vs M_{DM} after imposing the bounds from correct relic density of DM, direct and indirect detection of DM and search for B – L gauge boson at ATLAS which are shown in Fig.20. If we compare the plot of Fig. 18 and Fig. 19 with the plot of Fig.20, we can infer how much parameter space

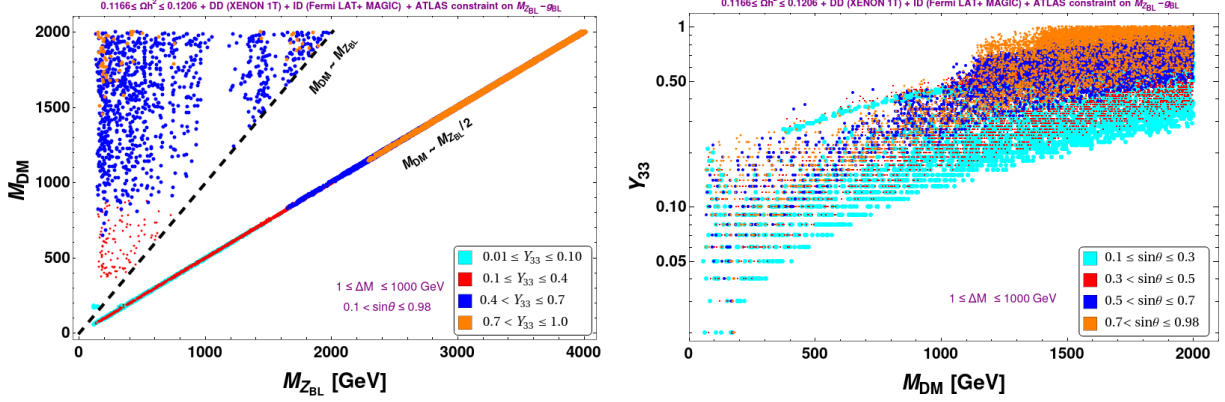


FIG. 20: Parameter space satisfying relic density, direct and indirect detection bound as well as $g_{BL} - M_{Z_{BL}}$ constraint from ATLAS is shown in the plane of M_{DM} vs $M_{Z_{BL}}$ (left) and Y_{33} vs M_{DM} (Right).

gets ruled out by the imposition of the constraints from ATLAS. We also show the parameter space satisfying correct relic, direct and indirect constraint along with the constraint from ATLAS on $g_{BL} - M_{Z_{BL}}$ in the plane of M_{DM} vs $M_{Z_{BL}}$ (left) and Y_{33} vs M_{DM} (right) in Fig 20. The points along the diagonal of the plot essentially corresponds to the points at the Z_{BL} resonance which occurs for $M_{DM} \sim M_{Z_{BL}}/2$. But as we can see clearly that apart from these points, all relevant constraints are also getting satisfied for a DM Mass range $M_{DM} > M_{Z_{BL}}$. This enhanced parameter space is the result of additional annihilation and co-annihilations possible in this considered model. The different colors of the points corresponds to different ranges of the Yukawa coupling Y_{33} . Clearly as the DM mass increases, a larger Y_{33} can lead to correct relic as well as all other constraints discussed in this context.

V. COLLIDER SIGNATURE OF DOUBLY CHARGED SCALAR IN PRESENCE OF Z_{BL}

The light doubly charged scalar in this model offers novel multi-lepton signatures with missing energy and jets. It is worthy to mention here that the dark sector which contains the gauge singlet Majorana fermions do not have any promising collider signatures as the mono-X type signal processes, arising out of initial state radiation are extremely suppressed. The doubly charged scalar, $H^{\pm\pm}$ which is also charged under $U(1)_{B-L}$ can be produced at Large Hadron Collider (LHC) via Higgs ($H_{1,2,3}$) and gauge bosons (γ, Z, Z_{BL}) mediations.

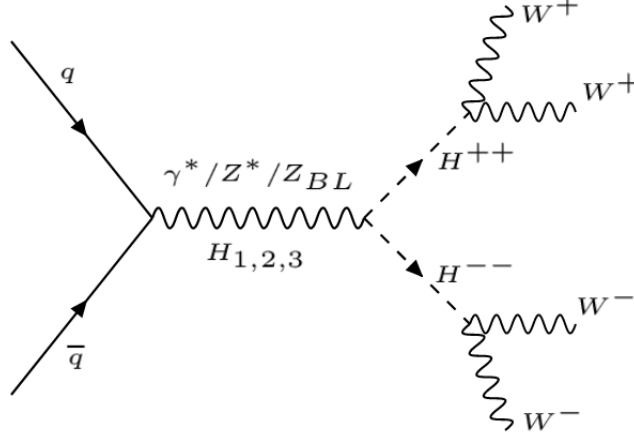


FIG. 21: Feynman diagram for pair production of doubly charged scalar at LHC via Higgs ($H_{1,2,3}$) and Gauge Bosons (γ, Z, Z_{BL}) mediations.

Further decay of $H^{\pm\pm}$ to $W^\pm W^\pm$ pair (assumed $m_{H^{\pm\pm}} \geq 2m_W$) with almost 100% branching ratio for $v_\xi \sim 2.951$ GeV yields $W^+W^+W^-W^-$ final state. As a result the four W final state offers: $4\ell + \cancel{E}_T$ and $m\ell + nj + \cancel{E}_T$ signatures at collider. For details of branching fraction and partial decay widths of H^{++} with v_ξ , please see appendix B. Although this type of signatures have been studied in the context of Type -II see-saw model, the triplet scalar ξ considered in this model also have $U(1)_{B-L}$ charge on top SM gauge charges and that makes this model different from the usual type-II seesaw scenario. In this section we will briefly highlight the effect of additional gauge boson Z_{BL} on the pair production cross-section of doubly charged scalar. The corresponding Feynman diagram of this type process is shown in Fig.21.

The pair production cross-section of doubly charged scalar, $H^{++}H^{--}$ as function of mass, $m_{H^{\pm\pm}}$ for fixed value of $M_{Z_{BL}} = 4.5$ TeV with $\sqrt{s} = 13$ TeV is shown in Fig.22. The production cross-sections are computed in `MicrOmegas` using the NNPDF23 parton distributions. The black solid line corresponds to the case where $U(1)_{B-L}$ gauge boson, Z_{BL} is absent and the scenario resembles the usual type-II see-saw scenario. And in that case the $H^{++}H^{--}$ pair can be produced via SM Higgs and SM gauge boson (γ, Z) mediated Drell-Yan processes. However in a gauged B – L scenario, the presence of the additional gauge boson Z_{BL} can affect this pair production cross-section of $H^{++}H^{--}$. The effects of $U(1)_{B-L}$ gauge boson on top of SM gauge bosons are shown by dotted lines in the Fig.22 for two different values of gauge couplings: $g_{BL} = 0.44$ (purple line) and 0.55 (blue line). It is important to

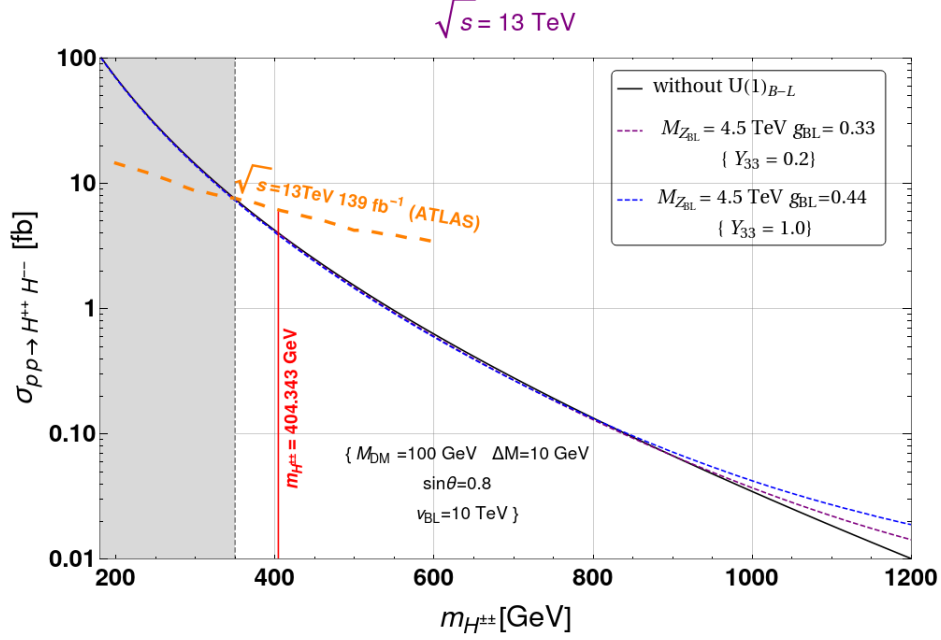


FIG. 22: Production cross-section for $pp \rightarrow H^{++} H^{--}$ as a function of doubly charged scalar mass $m_{H^{\pm\pm}}$ considering $\text{Br}(H^{\pm\pm} \rightarrow W^{\pm}W^{\pm}) \sim 100\%$ at $\sqrt{s} = 14$ TeV. The black solid line corresponds to the usual type-II seesaw scenario where Z_{BL} gauge mediated diagrams are absent. The effects of Z_{BL} on the production cross-section are shown dashed in dashed lines: purple line ($M_{Z_{BL}} = 4.5$ TeV, $g_{BL} = 0.44$) and blue line ($M_{Z_{BL}} = 4.5$ TeV, $g_{BL} = 0.55$). Other parameters are fixed as mentioned inset of the figure. The shaded region is excluded from ATLAS data on doubly charged scalar mass, $m_{H^{\pm\pm}}$ for $\sqrt{s} = 13$ TeV and luminosity 139 fb^{-1} .

note here that the above values of the g_{BL} can be obtained using the Eqn.28 keeping the other parameters fixed as mentioned in the inset of the figure. For illustration purpose we considered two moderate values of g_{BL} : 0.44 (purple dashed line) and 0.55 (blue dashed line) which are in agreement with the current ATLAS bound $g_{BL} \leq 0.57$ for $M_{Z_{BL}} = 4.5$ TeV. It is noticeable from the graph that the presence of Z_{BL} enhances the production cross-section towards the heavy mass region of doubly charge scalar with moderate value of g_{BL} compared to the case without $U(1)_{B-L}$ augmentation. It is because of the on-shell decay of Z_{BL} to $H^{++}H^{--}$ pair as $M_{Z_{BL}} > 2m_{H^{\pm\pm}}$ and there is a constructive interference between Z_{BL} and the SM gauge bosons. The orange dashed line shows the observed and expected upper limit on $H^{++}H^{--}$ pair production cross-section as a function of doubly charged scalar mass $m_{H^{\pm\pm}}$ at 95% CL which is obtained from the combination of multi-leptons with jets plus missing

energy search at ATLAS with $\sqrt{s} = 13\text{TeV}$ and integrated luminosity, $\mathcal{L} = 139\text{ fb}^{-1}$ [85]. This upper limit of production cross-section excludes the region of doubly charged triplet mass, $m_{H^{\pm\pm}} \leq 350\text{ GeV}$ as shown by the shaded region in Fig.22.

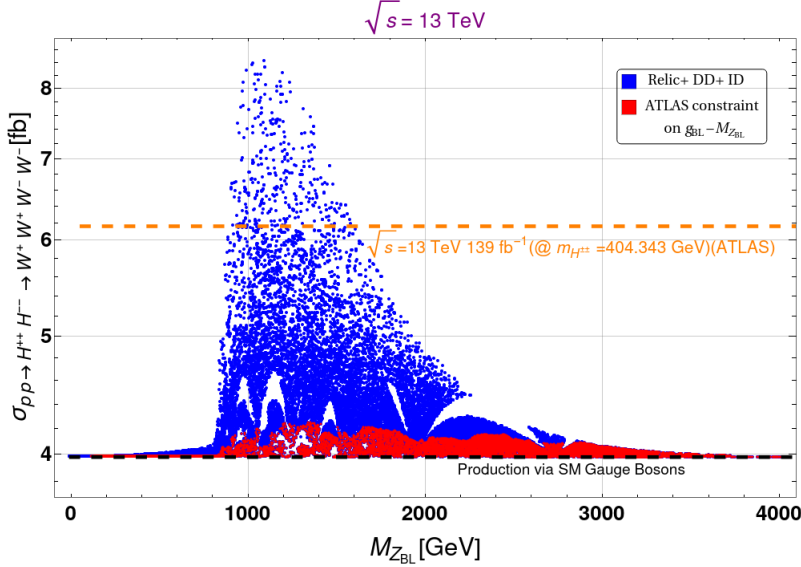


FIG. 23: The model parameters are projected against the production cross-section of doubly charged scalar ($H^{\pm\pm}$) as a function of B – L gauge boson mass $M_{Z_{BL}}$. The blue points are satisfying the Relic+Direct Detection+ Indirect Detection constraints. Red points are consistent with the ATLAS constraint on $g_{BL} - M_{Z_{BL}}$.

In figure 23, we projected the points satisfying all the relevant constraints against the doubly charged scalar ($H^{\pm\pm}$) production cross-section as a function of B – L gauge boson mass $M_{Z_{BL}}$ with $\sqrt{s} = 13\text{ TeV}$ for a benchmark value of $m_{H^{\pm\pm}} = 404.343\text{ GeV}$. The orange dashed line shows the upper limit on the production cross-section from ATLAS [85]. The blue points show the parameters that satisfy all the relevant constraints like correct relic density, direct and indirect search of DM. We can see that in presence of the B – L gauge boson, the production cross-section $\sigma_{pp \rightarrow H^{++}H^{--}}$ can get a distinctive enhancement as compared to the case where production of $H^{\pm\pm}$ happens through SM gauge bosons (γ^*, Z^*) mediation only which is shown as the dashed black line for easy comparison. But since the gauge coupling, g_{BL} is strongly constrained for a corresponding value of $M_{Z_{BL}}$ from non-observation of new gauge boson at LHC, when we impose this constraint on $g_{BL} - M_{Z_{BL}}$, we see that there is not much enhancement in the production cross-section as compared to the SM. It is clear from the red colored points in fig 23 that even in the presence of additional gauge boson Z_{BL} , we

can see only a 5% enhancement (i.e $\sigma_{pp \rightarrow H^{++}H^{--}} = 4.2$ fb in presence of Z_{BL} as compared to 4 fb predicted by SM.) in the production of the doubly charged scalar of mass around 400 GeV. Thus it is conclusive to say that the contribution from Z_{BL} mediated production is negligible as compared to the SM gauge boson mediation for $m_{H^{\pm\pm}} \sim 350 - 800$ GeV or so.

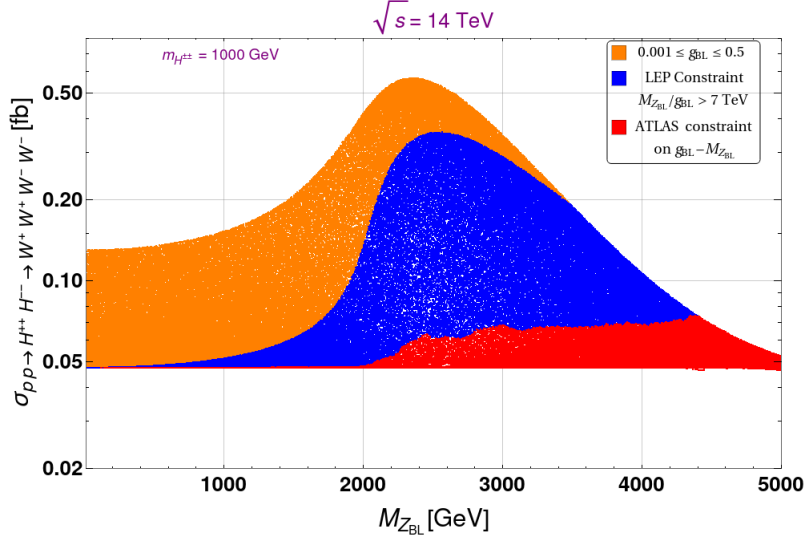


FIG. 24: The production cross-section of doubly charged scalar ($H^{\pm\pm}$) as a function of $M_{Z_{BL}}$. The orange points correspond to gauge coupling: $0.001 \leq g_{BL} \leq 0.50$. The blue points are allowed from LEP exclusion bound. Red points are consistent with ATLAS constraint on $g_{BL} - M_{Z_{BL}}$.

However if we consider the doubly charged scalar mass in the TeV scale, requiring a higher $M_{Z_{BL}}$ (> 2 TeV) for the resonance enhancement to happen, we can see a perceptible signal at the collider. Thus to demonstrate this fact, we considered the doubly charged scalar mass $m_{H^{\pm\pm}} = 1$ TeV. In figure 24, we show the production cross-section of doubly charged scalar ($H^{\pm\pm}$) as a function of $M_{Z_{BL}}$ considering the gauge coupling within the interval $0.001 \leq g_{BL} \leq 0.50$ with $\sqrt{s} = 14$ TeV shown by the orange points. Though the constraints from the current LHC experiments have already surpassed the LEP II limits on $g_{BL} - M_{Z_{BL}}$, for comparison we show the blue points in the plot which depicts the maximum increase in $\sigma_{pp \rightarrow H^{++}H^{--}}$ when the constraint from LEP on $g_{BL} - M_{Z_{BL}}$ is incorporated into the calculation. However, even after imposing the most stringent constraint from ATLAS on $g_{BL} - M_{Z_{BL}}$, we observe that there is noteworthy enhancement in the production of $H^{\pm\pm}$ as compared to the value predicted by SM. The production cross-section $\sigma_{pp \rightarrow H^{++}H^{--}}$ increases

by almost 34% (0.063 fb in presence of Z_{BL} as compared to 0.047 fb predicted by SM) for $M_{Z_{BL}}$ around 2.5 TeV and it further gets enhanced by almost 54% (0.074 fb in presence of Z_{BL} as compared to 0.047 fb predicted by SM) if $M_{Z_{BL}}$ is around 4.4 TeV. This feature is evident from the red points in fig 24. This is the crucial evidence of the scenario considered here that can be probed by the near and future colliders and hence the feasibility of this model can be verified.

This also establishes an interesting connection between the dark sector and the generation of neutrino mass via the modified type-II seesaw in a gauged $B - L$ setup that we discussed.

VI. CONCLUSION

In this paper, we have studied a very well motivated gauge extension of the standard model by augmenting the SM gauge group with a $U(1)_{B-L}$ symmetry which happens to be an accidental symmetry of SM to simultaneously address non-zero masses and of light neutrinos as well as a phenomenologically viable dark matter component of the universe. The neutrino mass is explained through an alternative type-II see-saw mechanism by incorporating two scalar triplets in the model, one being super heavy and the other in the TeV scale and thus having the potential to be detected at present and future colliders through its interesting signatures. We minimally extend the fermion particle content of the model by adding three exotic right chiral fermions χ_{i_R} with $B - L$ charges $-4, -4$ and $+5$ in order to cancel the gauge and gravitational anomalies that arise when one gauges the $B - L$ symmetry. The stability of these fermions is owed to the remnant \mathcal{Z}_2 symmetry after the $U(1)_{B-L}$ breaking which distinguishes the added fermions from the SM as $\chi'_{i_R}s$ are odd under \mathcal{Z}_2 while all other particles are even. Thus the dark matter emerges as the lightest Majorana fermion from the mixture of these exotic fermions.

A very interesting and important aspect of the model is the correlation between neutrino mass and dark sector. As generation of neutrino mass is explained through a modified type-II seesaw at TeV scale by introducing two $SU(2)_L$ triplet scalars Δ and ξ . Δ is super heavy and doesn't have a coupling with the lepton and hence can not generate the neutrino mass even after acquiring an induced vev after the EW symmetry breaking. Thus the neutrino mass is essentially generated through the ξLL coupling as given in Eq. 11. In the limit $v_{BL} \rightarrow 0$, which essentially means vanishing mixing between Δ and ξ , the neutrino mass also vanishes.

Also Eqs. 3, 22 and 24 implies that the interaction between χ_{τ_R} and χ_{e_R}, χ_{μ_R} is established through the scalar Φ_{BL} . In the limit of $\langle \Phi_{BL} \rangle \rightarrow 0$, which essentially implies $\sin \theta \rightarrow 0$, the DM candidate χ_3 decouples from the heavier dark particles χ_1 and χ_2 . In this limit there will be no co-annihilations among the dark sector particles. Thus only if $\langle \Phi_{BL} \rangle \neq 0$, we get non-zero masses of light neutrinos as well as it switches on the co-annihilations of DM and hence enlarges the parameter space satisfying all relevant constraints.

We studied the model parameter space by taking into account all annihilation and co-annihilation channels for DM mass ranging from 1 GeV to 2 TeV. We confronted our results with recent data from PLANCK and XENON-1T to obtain the parameter space satisfying relic density as well as direct detection constraints. The DM being Majorana in nature, it escapes from the gauge boson mediated direct detection constraint. We also checked for the constraints on our model parameters from the indirect search of DM using the recent data from Fermi-LAT and MAGIC which we found to be relatively weaker than other constraints. We also imposed the constraint on $g_{BL} - M_{Z_{BL}}$ from current LHC data to obtain the final parameter space allowed from all constraints including correct relic, direct and indirect detection of DM as well as the constraints from colliders on the B – L gauge boson and the corresponding coupling.

We also studied the detection prospects of the doubly charged scalar triplet which can have novel signatures at the colliders with multi-leptons along with missing energy and jets. We showed how in the presence of the B – L gauge boson Z_{BL} , the pair production cross-section of $H^{++}H^{--}$ can get enhanced and also depicted how the dark parameters satisfying all the relevant constraints can affect the production of this doubly charged scalar.

Acknowledgments

SM would like to acknowledge Alexander Belyaev and Alexander Pukhov for useful discussions. PG would like to acknowledge the support from DAE, India for the Regional Centre for Accelerator based Particle Physics (RECAPP), Harish Chandra Research Institute.

Appendix A: Anomaly Cancellation

In any chiral gauge theory the anomaly coefficient is given by [86]:

$$\mathcal{A} = \text{Tr}[T_a[T_b, T_c]_+]_R - \text{Tr}[T_a[T_b, T_c]_+]_L, \quad (\text{A1})$$

where T denotes the generators of the gauge group and R, L represent the interactions of right and left chiral fermions with the gauge bosons.

Gauging of $U(1)_{B-L}$ symmetry within the SM lead to the following triangle anomalies:

$$\mathcal{A}_1[U(1)_{B-L}^3] = 3$$

$$\mathcal{A}_2[(Gravity)^2 \times U(1)_{B-L}] = 3. \quad (\text{A2})$$

The natural choice to make the gauged B–L model anomaly free is by introducing three right handed neutrinos, each of having B–L charge -1 such that they result in $\mathcal{A}_1[U(1)_{B-L}^3] = -3$ and $\mathcal{A}_2[(Gravity)^2 \times U(1)_{B-L}] = -3$ which lead to cancellation of above mentioned gauge anomalies.

However we can have alternative ways of constructing anomaly free versions of $U(1)_{B-L}$ extension of the SM. In particular, three right chiral fermions with exotic B – L charges $-4, -4, +5$ can also give rise to vanishing B – L anomalies.

$$\mathcal{A}_1[U(1)_{B-L}^3] = \mathcal{A}_1^{SM}[U(1)_{B-L}^3] + \mathcal{A}_1^{New}[U(1)_{B-L}^3] = 3 + [(-4)^3 + (-4)^3 + (5)^3] = 0$$

$$\begin{aligned} \mathcal{A}_2[(Gravity)^2 \times U(1)_{B-L}] &= \mathcal{A}_2^{SM}[(Gravity)^2 \times U(1)_{B-L}] + \mathcal{A}_2^{New}[(Gravity)^2 \times U(1)_{B-L}] \\ &= 3 + [(-4) + (-4) + (5)] = 0 \end{aligned} \quad (\text{A3})$$

Appendix B: Decay of Doubly Charged Scalar

The partial decay widths of the doubly charged scalar(H^{++}) are given as:

$$\Gamma(H^{++} \rightarrow l_\alpha^+ l_\beta^+) = \frac{m_{H^{++}}}{4\pi v_\xi^2 (1 + \delta_{\alpha\beta})} |(M_\nu)_{\alpha\beta}|^2 \quad (\text{B1})$$

and

$$\Gamma(H^{++} \rightarrow W^+ W^+) = g^4 v_\xi^2 m_{H^{++}}^3 \left[1 - 4 \left(\frac{m_W}{m_{H^{++}}} \right)^2 \right]^{\frac{1}{2}} \left[1 - 4 \left(\frac{m_W}{m_{H^{++}}} \right)^2 + \left(\frac{m_W}{m_{H^{++}}} \right)^4 \right] \quad (\text{B2})$$

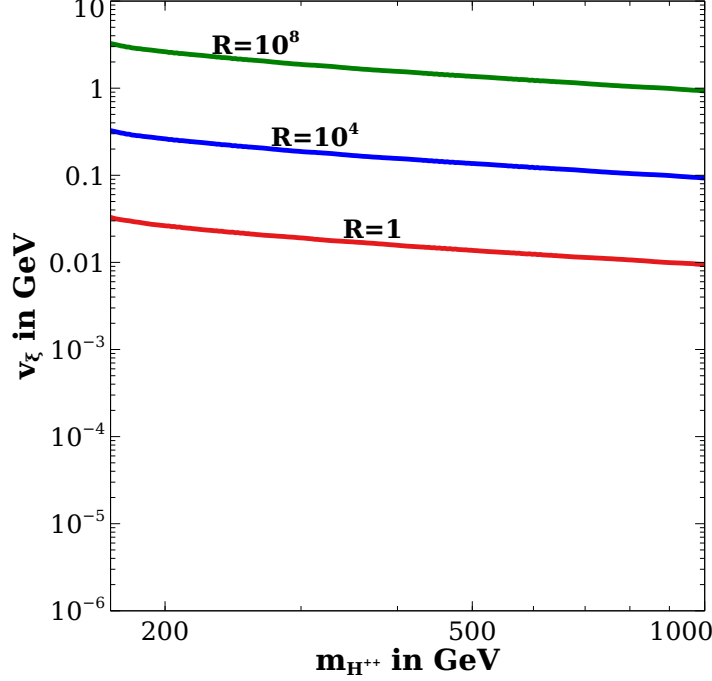


FIG. 25: The contour for R in the plane of v_ξ vs M_ξ .

This can be well analyzed by plotting contours of the ratio

$$R = \frac{\Gamma(H^{++} \rightarrow W^+W^+)}{\Gamma(H^{++} \rightarrow l_\alpha^+ l_\beta^+)} \quad (\text{B3})$$

in the plane of $m_{H^{++}}$ vs v_ξ as shown in the Fig. 25. It can be easily inferred from Fig 25 that if v_ξ is a few hundred MeV or more, then H^{++} dominantly decays to W^+W^+ .

-
- [1] G. Bertone, D. Hooper, and J. Silk, *Particle dark matter: Evidence, candidates and constraints*, *Phys. Rept.* **405** (2005) 279–390, [[hep-ph/0404175](#)].
 - [2] F. Zwicky, *Die Rotverschiebung von extragalaktischen Nebeln*, *Helv. Phys. Acta* **6** (1933) 110–127. [Gen. Rel. Grav.41,207(2009)].
 - [3] V. C. Rubin and W. K. Ford, Jr., *Rotation of the Andromeda Nebula from a Spectroscopic Survey of Emission Regions*, *Astrophys. J.* **159** (1970) 379–403.
 - [4] D. Clowe, M. Bradac, A. H. Gonzalez, M. Markevitch, S. W. Randall, C. Jones, and D. Zaritsky, *A direct empirical proof of the existence of dark matter*, *Astrophys. J.* **648** (2006) L109–L113, [[astro-ph/0608407](#)].

- [5] **WMAP** Collaboration, G. Hinshaw et al., *Nine-Year Wilkinson Microwave Anisotropy Probe (WMAP) Observations: Cosmological Parameter Results*, *Astrophys. J. Suppl.* **208** (2013) 19, [[arXiv:1212.5226](#)].
- [6] **Planck** Collaboration, N. Aghanim et al., *Planck 2018 results. VI. Cosmological parameters*, [arXiv:1807.06209](#).
- [7] E. W. Kolb and M. S. Turner, *The Early Universe*, *Front. Phys.* **69** (1990) 1–547.
- [8] G. Arcadi, M. Dutra, P. Ghosh, M. Lindner, Y. Mambrini, M. Pierre, S. Profumo, and F. S. Queiroz, *The Waning of the WIMP? A Review of Models, Searches, and Constraints*, [arXiv:1703.07364](#).
- [9] **LUX** Collaboration, D. S. Akerib et al., *Results from a search for dark matter in the complete LUX exposure*, *Phys. Rev. Lett.* **118** (2017), no. 2 021303, [[arXiv:1608.07648](#)].
- [10] **PandaX-II** Collaboration, A. Tan et al., *Dark Matter Results from First 98.7 Days of Data from the PandaX-II Experiment*, *Phys. Rev. Lett.* **117** (2016), no. 12 121303, [[arXiv:1607.07400](#)].
- [11] **PandaX-II** Collaboration, X. Cui et al., *Dark Matter Results From 54-Ton-Day Exposure of PandaX-II Experiment*, [arXiv:1708.06917](#).
- [12] **XENON** Collaboration, E. Aprile et al., *First Dark Matter Search Results from the XENON1T Experiment*, [arXiv:1705.06655](#).
- [13] **XENON** Collaboration, E. Aprile et al., *Dark Matter Search Results from a One Ton-Year Exposure of XENON1T*, *Phys. Rev. Lett.* **121** (2018), no. 11 111302, [[arXiv:1805.12562](#)].
- [14] **Fermi-LAT** Collaboration, M. Ackermann et al., *Searching for Dark Matter Annihilation from Milky Way Dwarf Spheroidal Galaxies with Six Years of Fermi Large Area Telescope Data*, *Phys. Rev. Lett.* **115** (2015), no. 23 231301, [[arXiv:1503.02641](#)].
- [15] **Fermi-LAT, MAGIC** Collaboration, M. L. Ahnen et al., *Limits to dark matter annihilation cross-section from a combined analysis of MAGIC and Fermi-LAT observations of dwarf satellite galaxies*, *JCAP* **1602** (2016), no. 02 039, [[arXiv:1601.06590](#)].
- [16] **Super-Kamiokande** Collaboration, Y. Fukuda et al., *Evidence for oscillation of atmospheric neutrinos*, *Phys. Rev. Lett.* **81** (1998) 1562–1567, [[hep-ex/9807003](#)].
- [17] **SNO** Collaboration, Q. R. Ahmad et al., *Measurement of the rate of $\nu_e + d \rightarrow p + p + e^-$ interactions produced by ^8B solar neutrinos at the Sudbury Neutrino Observatory*, *Phys. Rev. Lett.* **87** (2001) 071301, [[nucl-ex/0106015](#)].

- [18] **Double Chooz** Collaboration, Y. Abe et al., *Indication of Reactor $\bar{\nu}_e$ Disappearance in the Double Chooz Experiment*, *Phys. Rev. Lett.* **108** (2012) 131801, [[arXiv:1112.6353](#)].
- [19] **Daya Bay** Collaboration, F. P. An et al., *Observation of electron-antineutrino disappearance at Daya Bay*, *Phys. Rev. Lett.* **108** (2012) 171803, [[arXiv:1203.1669](#)].
- [20] **RENO** Collaboration, J. K. Ahn et al., *Observation of Reactor Electron Antineutrino Disappearance in the RENO Experiment*, *Phys. Rev. Lett.* **108** (2012) 191802, [[arXiv:1204.0626](#)].
- [21] **Particle Data Group** Collaboration, M. Tanabashi et al., *Review of Particle Physics*, *Phys. Rev.* **D98** (2018), no. 3 030001.
- [22] S. Vagnozzi, E. Giusarma, O. Mena, K. Freese, M. Gerbino, S. Ho, and M. Lattanzi, *Unveiling ν secrets with cosmological data: neutrino masses and mass hierarchy*, *Phys. Rev. D* **96** (2017), no. 12 123503, [[arXiv:1701.08172](#)].
- [23] E. Giusarma, M. Gerbino, O. Mena, S. Vagnozzi, S. Ho, and K. Freese, *Improvement of cosmological neutrino mass bounds*, *Phys. Rev. D* **94** (2016), no. 8 083522, [[arXiv:1605.04320](#)].
- [24] E. Giusarma, S. Vagnozzi, S. Ho, S. Ferraro, K. Freese, R. Kamen-Rubio, and K.-B. Luk, *Scale-dependent galaxy bias, CMB lensing-galaxy cross-correlation, and neutrino masses*, *Phys. Rev. D* **98** (2018), no. 12 123526, [[arXiv:1802.08694](#)].
- [25] I. Esteban, M. C. Gonzalez-Garcia, A. Hernandez-Cabezudo, M. Maltoni, and T. Schwetz, *Global analysis of three-flavour neutrino oscillations: synergies and tensions in the determination of θ_{23} , δ_{CP} , and the mass ordering*, *JHEP* **01** (2019) 106, [[arXiv:1811.05487](#)].
- [26] P. Minkowski, $\mu \rightarrow e\gamma$ at a Rate of One Out of 10^9 Muon Decays?, *Phys. Lett.* **B67** (1977) 421–428.
- [27] M. Gell-Mann, P. Ramond, and R. Slansky, *Complex Spinors and Unified Theories*, *Conf. Proc.* **C790927** (1979) 315–321, [[arXiv:1306.4669](#)].
- [28] R. N. Mohapatra and G. Senjanovic, *Neutrino Mass and Spontaneous Parity Violation*, *Phys. Rev. Lett.* **44** (1980) 912.
- [29] J. Schechter and J. W. F. Valle, *Neutrino Masses in $SU(2) \times U(1)$ Theories*, *Phys. Rev.* **D22** (1980) 2227.
- [30] R. N. Mohapatra and G. Senjanovic, *Neutrino Masses and Mixings in Gauge Models with*

- Spontaneous Parity Violation*, *Phys. Rev.* **D23** (1981) 165.
- [31] G. Lazarides, Q. Shafi, and C. Wetterich, *Proton Lifetime and Fermion Masses in an $SO(10)$ Model*, *Nucl. Phys.* **B181** (1981) 287–300.
 - [32] J. Schechter and J. W. F. Valle, *Neutrino Decay and Spontaneous Violation of Lepton Number*, *Phys. Rev.* **D25** (1982) 774.
 - [33] C. Wetterich, *Neutrino Masses and the Scale of B - L Violation*, *Nucl. Phys.* **B187** (1981) 343–375.
 - [34] B. Brahmachari and R. N. Mohapatra, *Unified explanation of the solar and atmospheric neutrino puzzles in a minimal supersymmetric $SO(10)$ model*, *Phys. Rev.* **D58** (1998) 015001, [[hep-ph/9710371](#)].
 - [35] R. Foot, H. Lew, X. G. He, and G. C. Joshi, *Seesaw Neutrino Masses Induced by a Triplet of Leptons*, *Z. Phys.* **C44** (1989) 441.
 - [36] S. Weinberg, *Baryon and Lepton Nonconserving Processes*, *Phys. Rev. Lett.* **43** (1979) 1566–1570.
 - [37] E. Ma, *Pathways to naturally small neutrino masses*, *Phys. Rev. Lett.* **81** (1998) 1171–1174, [[hep-ph/9805219](#)].
 - [38] J. McDonald, N. Sahu, and U. Sarkar, *Type-II Seesaw at Collider, Lepton Asymmetry and Singlet Scalar Dark Matter*, *JCAP* **04** (2008) 037, [[arXiv:0711.4820](#)].
 - [39] P.-H. Gu, H.-J. He, U. Sarkar, and X.-m. Zhang, *Double Type-II Seesaw, Baryon Asymmetry and Dark Matter for Cosmic e^\pm Excesses*, *Phys. Rev. D* **80** (2009) 053004, [[arXiv:0906.0442](#)].
 - [40] S. K. Majee and N. Sahu, *Dilepton Signal of a Type-II Seesaw at CERN LHC: Reveals a TeV Scale B - L Symmetry*, *Phys. Rev. D* **82** (2010) 053007, [[arXiv:1004.0841](#)].
 - [41] K. Huitu, J. Maalampi, A. Pietila, and M. Raidal, *Doubly charged Higgs at LHC*, *Nucl. Phys. B* **487** (1997) 27–42, [[hep-ph/9606311](#)].
 - [42] E. J. Chun, K. Y. Lee, and S. C. Park, *Testing Higgs triplet model and neutrino mass patterns*, *Phys. Lett.* **B566** (2003) 142–151, [[hep-ph/0304069](#)].
 - [43] P. Fileviez Perez, T. Han, G.-y. Huang, T. Li, and K. Wang, *Neutrino Masses and the CERN LHC: Testing Type II Seesaw*, *Phys. Rev.* **D78** (2008) 015018, [[arXiv:0805.3536](#)].
 - [44] R. Padhan, D. Das, M. Mitra, and A. Kumar Nayak, *Probing doubly and singly charged Higgs bosons at the pp collider HE -LHC*, *Phys. Rev. D* **101** (2020), no. 7 075050,

- [arXiv:1909.10495].
- [45] P. S. Bhupal Dev and Y. Zhang, *Displaced vertex signatures of doubly charged scalars in the type-II seesaw and its left-right extensions*, *JHEP* **10** (2018) 199, [arXiv:1808.00943].
 - [46] B. Barman, S. Bhattacharya, P. Ghosh, S. Kadam, and N. Sahu, *Fermion Dark Matter with Scalar Triplet at Direct and Collider Searches*, arXiv:1902.01217.
 - [47] S. Bhattacharya, P. Ghosh, N. Sahoo, and N. Sahu, *A Mini-review on Vector-like Leptonic Dark Matter, Neutrino Mass and Collider Signatures*, arXiv:1812.06505.
 - [48] J. C. Montero and V. Pleitez, *Gauging $U(1)$ symmetries and the number of right-handed neutrinos*, *Phys. Lett.* **B675** (2009) 64–68, [arXiv:0706.0473].
 - [49] B. L. Sánchez-Vega, J. C. Montero, and E. R. Schmitz, *Complex Scalar DM in a B - L Model*, *Phys. Rev.* **D90** (2014), no. 5 055022, [arXiv:1404.5973].
 - [50] E. Ma and R. Srivastava, *Dirac or inverse seesaw neutrino masses with $B - L$ gauge symmetry and S_3 flavor symmetry*, *Phys. Lett.* **B741** (2015) 217–222, [arXiv:1411.5042].
 - [51] B. L. Sánchez-Vega and E. R. Schmitz, *Fermionic dark matter and neutrino masses in a B - L model*, *Phys. Rev.* **D92** (2015) 053007, [arXiv:1505.03595].
 - [52] E. Ma, N. Pollard, R. Srivastava, and M. Zakeri, *Gauge $B - L$ Model with Residual Z_3 Symmetry*, *Phys. Lett.* **B750** (2015) 135–138, [arXiv:1507.03943].
 - [53] S. Patra, W. Rodejohann, and C. E. Yaguna, *A new $B - L$ model without right-handed neutrinos*, *JHEP* **09** (2016) 076, [arXiv:1607.04029].
 - [54] D. Nanda and D. Borah, *Common origin of neutrino mass and dark matter from anomaly cancellation requirements of a $U(1)_{B-L}$ model*, *Phys. Rev.* **D96** (2017), no. 11 115014, [arXiv:1709.08417].
 - [55] P.-H. Gu, *Double type-II Dirac seesaw accompanied by Dirac fermionic dark matter*, arXiv:1907.11557.
 - [56] N. Okada, S. Okada, and D. Raut, *A natural Z' -portal Majorana dark matter in alternative $U(1)$ extended Standard Model*, *Phys. Rev.* **D100** (2019), no. 3 035022, [arXiv:1811.11927].
 - [57] S. Mahapatra, N. Narendra, and N. Sahu, *Verifiable type-II seesaw and dark matter in a gauged $U(1)_{B-L}$ model*, arXiv:2002.07000.
 - [58] K. Asai, K. Nakayama, and S.-Y. Tseng, *Alternative minimal $U(1)_{BL}$* , *Phys. Lett. B* **814** (2021) 136106, [arXiv:2011.10365].
 - [59] J. G. Rodrigues, A. C. O. Santos, J. G. Ferreira Jr, and C. A. de S. Pires, *Neutrino masses*,

- cosmological inflation and dark matter in a variant $U(1)_{B-L}$ model with type II seesaw mechanism*, *Chin. Phys. C* **45** (2021), no. 2 025110, [[arXiv:1807.02204](#)].
- [60] D. Borah, D. Nanda, N. Narendra, and N. Sahu, *Right-handed Neutrino Dark Matter with Radiative Neutrino Mass in Gauged $B-L$ Model*, [arXiv:1810.12920](#).
- [61] N. Okada and S. Okada, *Z' -portal right-handed neutrino dark matter in the minimal $U(1)_X$ extended Standard Model*, *Phys. Rev. D* **95** (2017), no. 3 035025, [[arXiv:1611.02672](#)].
- [62] D. Nanda and D. Borah, *Connecting Light Dirac Neutrinos to a Multi-component Dark Matter Scenario in Gauged $B-L$ Model*, *Eur. Phys. J. C* **80** (2020), no. 6 557, [[arXiv:1911.04703](#)].
- [63] R. N. Mohapatra and R. E. Marshak, *Local $B-L$ Symmetry of Electroweak Interactions, Majorana Neutrinos and Neutron Oscillations*, *Phys. Rev. Lett.* **44** (1980) 1316–1319. [Erratum: *Phys. Rev. Lett.* 44,1643(1980)].
- [64] R. E. Marshak and R. N. Mohapatra, *Quark - Lepton Symmetry and $B-L$ as the $U(1)$ Generator of the Electroweak Symmetry Group*, *Phys. Lett.* **91B** (1980) 222–224.
- [65] A. Masiero, J. F. Nieves, and T. Yanagida, *$B-l$ Violating Proton Decay and Late Cosmological Baryon Production*, *Phys. Lett.* **116B** (1982) 11–15.
- [66] R. N. Mohapatra and G. Senjanovic, *Spontaneous Breaking of Global $B-l$ Symmetry and Matter - Antimatter Oscillations in Grand Unified Theories*, *Phys. Rev.* **D27** (1983) 254.
- [67] W. Buchmuller, C. Greub, and P. Minkowski, *Neutrino masses, neutral vector bosons and the scale of $B-L$ breaking*, *Phys. Lett.* **B267** (1991) 395–399.
- [68] A. Arhrib, R. Benbrik, M. Chabab, G. Moulhaka, M. C. Peyranere, L. Rahili, and J. Ramadan, *The Higgs Potential in the Type II Seesaw Model*, *Phys. Rev.* **D84** (2011) 095005, [[arXiv:1105.1925](#)].
- [69] S. Bhattacharya, N. Sahoo, and N. Sahu, *Singlet-Doublet Fermionic Dark Matter, Neutrino Mass and Collider Signatures*, *Phys. Rev.* **D96** (2017), no. 3 035010, [[arXiv:1704.03417](#)].
- [70] T. Robens and T. Stefaniak, *Status of the Higgs Singlet Extension of the Standard Model after LHC Run 1*, *Eur. Phys. J. C* **75** (2015) 104, [[arXiv:1501.02234](#)].
- [71] G. Chalons, D. Lopez-Val, T. Robens, and T. Stefaniak, *The Higgs singlet extension at LHC Run 2*, *PoS ICHEP2016* (2016) 1180, [[arXiv:1611.03007](#)].
- [72] D. López-Val and T. Robens, *Δr and the W -boson mass in the singlet extension of the standard model*, *Phys. Rev.* **D90** (2014) 114018, [[arXiv:1406.1043](#)].

- [73] M. Dutta, S. Bhattacharya, P. Ghosh, and N. Sahu, *Singlet-Doublet Majorana Dark Matter and Neutrino Mass in a minimal Type-I Seesaw Scenario*, *JCAP* **03** (2021) 008, [[arXiv:2009.00885](#)].
- [74] K. Griest and D. Seckel, *Three exceptions in the calculation of relic abundances*, *Phys. Rev. D* **43** (1991) 3191–3203.
- [75] A. Chatterjee and N. Sahu, *Resurrecting L-type sneutrino dark matter in light of neutrino masses and LUX data*, *Phys. Rev. D* **90** (2014), no. 9 095021, [[arXiv:1407.3030](#)].
- [76] S. Patra, N. Sahoo, and N. Sahu, *Dipolar dark matter in light of the 3.5 keV x-ray line, neutrino mass, and LUX data*, *Phys. Rev. D* **91** (2015), no. 11 115013, [[arXiv:1412.4253](#)].
- [77] G. Belanger, F. Boudjema, A. Pukhov, and A. Semenov, *Dark matter direct detection rate in a generic model with micrOMEGAs 2.2*, *Comput. Phys. Commun.* **180** (2009) 747–767, [[arXiv:0803.2360](#)].
- [78] A. Semenov, *LanHEP — A package for automatic generation of Feynman rules from the Lagrangian. Version 3.2*, *Comput. Phys. Commun.* **201** (2016) 167–170, [[arXiv:1412.5016](#)].
- [79] J. M. Alarcon, L. S. Geng, J. Martin Camalich, and J. A. Oller, *The strangeness content of the nucleon from effective field theory and phenomenology*, *Phys. Lett. B* **730** (2014) 342–346, [[arXiv:1209.2870](#)].
- [80] M. Carena, A. Daleo, B. A. Dobrescu, and T. M. P. Tait, *Z' gauge bosons at the Tevatron*, *Phys. Rev. D* **70** (2004) 093009, [[hep-ph/0408098](#)].
- [81] G. Cacciapaglia, C. Csaki, G. Marandella, and A. Strumia, *The Minimal Set of Electroweak Precision Parameters*, *Phys. Rev. D* **74** (2006) 033011, [[hep-ph/0604111](#)].
- [82] **ATLAS** Collaboration, M. Aaboud et al., *Search for new high-mass phenomena in the dilepton final state using 36.1 fb¹ of proton-proton collision data at $\sqrt{s} = 13$ TeV with the ATLAS detector*, [arXiv:1707.02424](#).
- [83] **ATLAS** Collaboration, G. Aad et al., *Search for high-mass dilepton resonances using 139 fb¹ of pp collision data collected at $\sqrt{s} = 13$ TeV with the ATLAS detector*, *Phys. Lett. B* **796** (2019) 68–87, [[arXiv:1903.06248](#)].
- [84] **CMS** Collaboration, A. M. Sirunyan et al., *Search for high-mass resonances in dilepton final states in proton-proton collisions at $\sqrt{s} = 13$ TeV*, *JHEP* **06** (2018) 120, [[arXiv:1803.06292](#)].
- [85] **ATLAS** Collaboration, G. Aad et al., *Search for doubly and singly charged Higgs bosons*

decaying into vector bosons in multi-lepton final states with the ATLAS detector using proton-proton collisions at $\sqrt{s} = 13$ TeV, [arXiv:2101.11961](#).

- [86] P. Pal, *An Introductory Course of Particle Physics.*, CRC Press, Taylor & Francis Group.